Materials Today Bio 27 (2024) 101127

Contents lists available at ScienceDirect

Materials Today Bio

journal homepage: www.journals.elsevier.com/materials-today-bio

Cell-recruited microspheres for OA treatment by dual-modulating inflammatory and chondrocyte metabolism

Yun Zhou [a,1], Xu He [a,1], Wen Zhang [a,1], Weiguo Zhang [b], Huan Zhao [a], Xichao Zhou [a], Qiaoli Gu [a], Hao Shen [a], Huilin Yang [a], Xingzhi Liu [c,**], Lixin Huang [a,***], Qin Shi [a,*]

[a] Department of Orthopedics, The First Affiliated Hospital of Soochow University, Medical College of Soochow University, Orthopedic Institute of Soochow University, 899 Pinghai Road, Suzhou, Jiangsu, 215031, PR China

[b] Department of Radiology, Dushu Lake Hospital Affiliated to Soochow University, Medical Center of Soochow University, 9 Chongwen Road, Suzhou, Jiangsu, 215123, PR China

[c] CAS Key Laboratory of Nano-Bio Interface, Suzhou Institute of Nano-Tech and Nano-Bionics, Chinese Academy of Sciences, 398 Ruoshui Road, Suzhou, Jiangsu, 215123, PR China

ARTICLE INFO

Keywords:
Osteoarthritis
Hydrogel microspheres
Chondroitin sulfate
RGD
Transforming growth factor-β1

ABSTRACT

Osteoarthritis (OA) is a degenerative disease potentially exacerbated due to inflammation, cartilage degeneration, and increased friction. Both mesenchymal stem cells (MSCs) and pro-inflammatory macrophages play important roles in OA. A promising approach to treating OA is to modify multi-functional hydrogel microspheres to target the OA microenvironment and structure. Arginyl-glycyl-aspartic acid (RGD) is a peptide widely used in bioengineering owing to its cell adhesion properties, which can recruit BMSCs and macrophages. We developed TLC-R, a microsphere loaded with TGF-β1-containing liposomes. The recruitment effect of TLC-R on macrophages and BMSCs was verified by *in vitro* experiments, along with its function of promoting chondrogenic differentiation of BMSCs. And we evaluated the effect of TLC-R in balancing OA metabolism *in vitro* and *in vivo*. When TLC-R was co-cultured with BMSCs and lipopolysaccharide (LPS)-treated macrophages, it showed the ability to recruit both cells in substantial numbers. As the microspheres degraded, TGF-β1 and chondroitin sulfate (ChS) were released to promote chondrogenic differentiation of the recruited BMSCs, modulate chondrocyte metabolism and inhibit inflammation induced by the macrophages. Furthermore, *in vivo* analysis showed that TLC-R restored the narrowed space, reduced osteophyte volume, and improved cartilage metabolic homeostasis in OA rats. Altogether, TLC-R provides a comprehensive and novel solution for OA treatment by dual-modulating inflammatory and chondrocyte metabolism.

1. Introduction

Osteoarthritis (OA) is a widespread joint disease affecting more than 500 million people globally [1]. However, no efficient treatments are available for curing or alleviating OA [2]. The pathogenesis involves cartilage injury, inflammation, and lubrication [3]. The chondrogenic potential of mesenchymal stem cells (MSCs) makes them a promising candidate for cellular therapy of cartilage defects. We previously prepared a methacrylate gelatin (GelMA) scaffold loaded with bone mesenchymal stem cells (BMSCs) and TGF-β1 (GelMA-T/BMSCs) that demonstrated significant effectiveness at repairing nasal septal cartilage defects in rabbits [4]. However, exogenous BMSCs lose much of their self-renewal and differentiation abilities due to long-term *in vitro* culturing, so autologous BMSCs are preferable to allogeneic BMSCs [5]. However, autologous cell transplantation requires two invasive surgeries, which increases the burden on the patient and their risk of infection [6]. Therefore, finding a more straightforward approach to source autologous BMSCs for OA treatment is challenging.

One of the keys to OA inflammation is the dysregulation of macrophages [7], distributed in the knee joint among various tissues, such as

* Corresponding author.
** Corresponding author.
*** Corresponding author.
E-mail addresses: xzliu2019@sinano.ac.cn (X. Liu), szhuanglx@yeah.net (L. Huang), shiqin@suda.edu.cn (Q. Shi).
[1] These authors contributed equally to this paper.

https://doi.org/10.1016/j.mtbio.2024.101127
Received 20 February 2024; Received in revised form 6 June 2024; Accepted 12 June 2024
Available online 13 June 2024

the deep synovial tissues and ligaments [8,9]. In the case of OA, the synovium, which comprises lining and sub-lining layers, loses its integrity and results in uneven fibrous hyperplasia [10]. Concurrently, in OA, increased capillary permeability in the sub-lining layer accelerates drug excretion and reduces the duration of anti-inflammatory drugs in deep synovial tissues. Thus, drug penetration and targeted clearance of pro-inflammatory macrophages distributed in synovial tissues are particularly challenging [11]. Additionally, the disruption of lubrication between tissues in the knee joint is considered a critical mechanism in developing OA [12]. Thus, designing a multi-functional system that can simultaneously recruit autologous BMSCs and pro-inflammatory macrophages to promote lubrication, anti-inflammation, and cartilage regeneration and repair may be a promising therapeutic strategy for OA.

Arginyl-glycyl-aspartic acid (RGD) peptide is a short peptide comprising arginine, glycine, and aspartic acid that is a ligand specific to integrins on cell membranes and that plays an essential role in recruiting and adhering cells. RGD peptide has been used to modify hydrogels for various applications in bone tissue engineering [13,14]. For instance, RGD peptide can recruit MSCs by binding to the integrin α5β1 to repair bone defect sites [15]. RGD peptide can bind with the integrin αvβ3 to capture many macrophages [16]. However, RGD peptide is short without secondary or tertiary structures, so it lacks stability [17]. To overcome this drawback, RGD peptide is often loaded onto a scaffold in tissue engineering to endow the scaffold with unique properties and meet the therapeutic needs of various diseases. For example, Wang et al. developed a nanostructured bionic extracellular matrix (ECM) that promotes cell adhesion and osteoinduction by physically blending RGD peptide and Bone morphogenetic protein-2 (BMP-2) [18]. However, physical blending is not the ideal way for bioactive molecules to function because it may lead to the rapid release and easy metabolism of RGD peptide in the body [19]. Our group previously synthesized a photo-cross-linkable osteogenic growth peptide (OGP) and used GelMA as a template to construct a covalent photo-crosslinked hydrogel (GelMA-*c*-OGP) that prolongs the release time of OGP. Our composite hydrogel maintained the activity of OGP for an extended period and prolonged its release as the hydrogel degraded slowly [20]. We developed another GelMA/HSNGLPL (Pep-HGelMA) hydrogel by modifying GelMA with methacrylated HSNGLPL peptide having transforming growth factor-β1 (TGF-β1) affinity and showed that Pep-HGelMA preserves HSNGLPL for a long time, automatically recruits TGF-β1 and accelerates repair of cartilage tissue [21]. Therefore, peptides can be covalently linked to hydrogels to maintain structural stability and prolong their release time. By introducing acryloyl groups into the RGD peptides, forming RGDfk peptide acryloyl (Pep-RGDfkAC), they can also be coupled with double-bond modified photosensitive biomaterials under ultraviolet (UV) light and photoinitiators, thus maintaining the slow release and activity of RGD.

Scaffolds play a vital role in tissue engineering, and they are primarily made from natural or synthetic polymers [22]. However, the application of natural polymers as scaffolds is limited by their mechanical defects, high degradability, batch variance, difficult modification, and potential risks of immunogenicity and disease transmission [23,24]. Synthetic polymers can mimic the high water absorption of natural tissues, which are easy to adjust precisely and have low immunogenicity. Thus, they are often used as scaffolds with RGD peptide for tissue engineering [25]. Chondroitin Sulfate (ChS) is a natural glycosaminoglycan (≈500 Da), which is an important structural component of cartilage and other connective tissues, with many positive properties, such as promoting chondrogenic differentiation of BMSCs [26], fostering cartilage generation by balancing chondrocyte metabolism [27,28], promoting anti-inflammation [29], inhibiting cellular hypertrophy [30] and enhancing integration with natural cartilage [31]. However, ChS cannot be used alone to prepare scaffolds because of its good water solubility and inability to form a hydrogel by self-assembly. Methacrylated chondroitin sulfate (ChSMA) links methacrylate (MA) to the main chain of ChS, which can then form hydrogel scaffolds by binding with acryloyl groups in the presence of a suitable photoinitiator [32]. He et al. used electro-assisted printing to create ChSMA hydrogel microspheres anchored with liposome-encapsulated glycyrrhizin, which they applied to realize dual antioxidant actions [33]. However, this method cannot effectively control the size of microspheres. In contrast, microfluidics can produce ChSMA microspheres of uniform size that can simulate ball bearings [34,35], and liposomes can be introduced to further reduce surface friction and enhance the lubrication between tissues [36]. Moreover, such microspheres have a porous structure, so they possess high drug loading and release capabilities and thus are ideal drug carriers [37].

In this study, we modified ChS with methacrylic anhydride to prepare ChSMA, which coupled with Pep-RGDfkAC through acryloyl groups under UV light to obtain ChSMA-RGD microspheres. We then used amide groups to covalently bond hydrogenated soy phosphatidylcholine (HSPC)/cholesterol/1,2-Dioleoyl–SN–*glycero*-3-phosphoethanolamine (DOPE) liposomes (Lipo) loaded with TGF-β1 onto ChSMA-RGD to construct TGF-β1@Lipo@ChSMA-RGD microsphere (TLC-R). TLC-R is a multi-functional hydrogel microsphere that is simple to prepare and can prevent OA's degenerative progression (Scheme 1). The TLC-R acts as ball bearings to lubricate the joints. Meanwhile, TLC-R recruits MSCs and pro-inflammatory macrophages, followed by TGF-β1 promotes chondrogenic differentiation of MSCs, and the ChS attenuates the inflammatory response in pro-inflammatory macrophages. As TLC-R degrades, it releases ChS to further promote chondrocyte synthetic metabolism, and inhibit the degradation metabolism and inflammation over a long period. In summary, the TLC-R developed in this study is a simply prepared multifunctional system that can prevent the degenerative progression of OA.

2. Materials and methods

2.1. Synthesis and assay of ChSMA

First, 2 g of ChS was dissolved in 50 mL of phosphate buffered saline (PBS) (pH = 7.4). Then, 16.9 mL of methacrylic anhydride was added to the above solution under dark conditions (pH = 8.0). The solution was magnetically stirred for 2 h and was then placed in a refrigerator at 4 °C for 24 h. The solution was added with ethanol and stirred to precipitate a white flocculent precipitate, which was then dissolved with PBS and dialyzed for 2 weeks. Finally, ChSMA was obtained by freeze-drying. Nuclear magnetic resonance (NMR) (Bruker, Germany) and Fourier transform infrared spectroscopy (FTIR) (Thermo Science, USA) were used to determine whether MA was successfully modified.

2.2. Preparation and characterization of liposomes

TGF-β1@Lipo was prepared by the film dispersion method. Briefly, 50 ng of TGF-β1 (Novoprotein, China), 15 mg of HSPC, 5 mg of DOPE, 2 mg of octadecylamine, and 5 mg of cholesterol (Aladdin, China) were dissolved in 5 mL of trichloromethane. The mixed solution was evaporated in a rotary evaporator at 60 °C to form a lipid film. The liposome was then preheated and hydrated by adding 8 mL of double distilled water (ddH_2O) at 40 °C for 1 h and then sonicated for 20 min. Finally, TGF-β1@Lipo was obtained by sequential filtration through 450-nm and 220-nm polycarbonate membranes. Lipo was made similarly. The particle size and zeta potential of liposomes (Lipo, TGF-β1@Lipo) were detected by a nanoparticle analyzer (Malvern, UK). Transmission electron microscopy (TEM, Hitachi, Japan) was used to observe the morphology of the liposomes.

2.3. Preparation and characterization of microspheres

To produce ChSMA-RGD microspheres, 60 mg of ChSMA lyophilized hydrogel was dissolved in 1 mL of lithium phenyl-2,4,6-trimethylbenzoylphosphinate (LAP, EFL, China) and 2 mg of Pep-

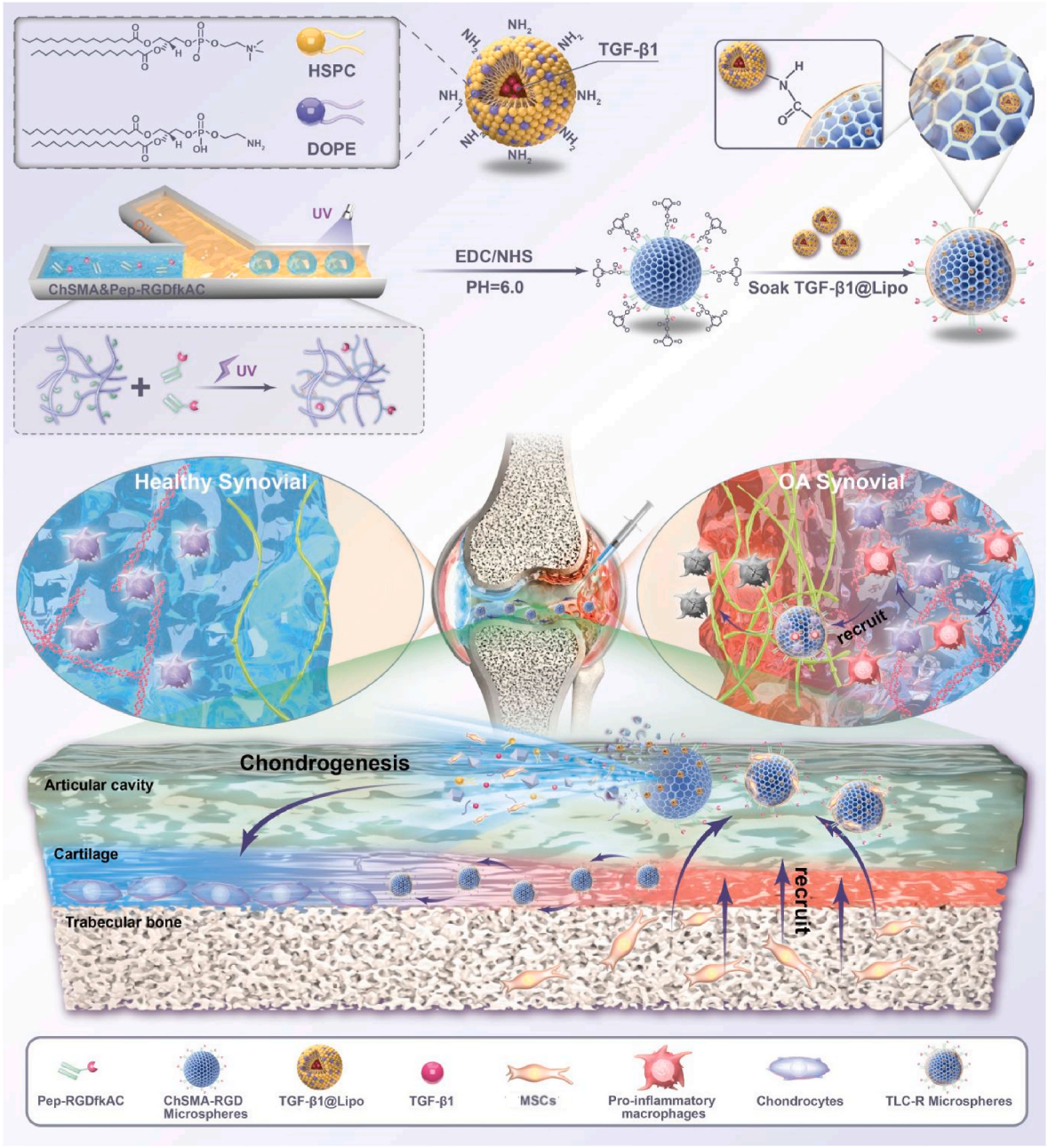

Scheme 1. Scheme of the production process of TLC-R and its application in OA treatment. TLC-R was fabricated by microfluidics and chemical crosslinking technologies. TLC-R can treat OA by recruiting pro-inflammatory macrophages and MSCs, reducing inflammation, promoting chondrogenic differentiation, modulating cartilage metabolism, and lubricating joints.

RGDfkAC (EFL, China) to obtain the aqueous-phase solution. The oil-phase solution was obtained by mixing isopropyl myristate (Aladdin, China) and dehydrated sorbitan oleate (Span 80, Aladdin, China). Single continuous droplets produced by a microfluidic device were collected and crosslinked by UV for 1 min. After washing, porous microspheres of ChSMA-RGD were formed by freeze-drying. ChSMA microspheres were prepared using the same method. The freeze-dried microspheres were re-solubilized with PBS and were then observed and photographed under an inverted fluorescence microscope (Zeiss, Germany). The particle size was counted by ImageJ. The surface morphology of the freeze-dried microspheres was photographed by scanning electron microscopy (SEM, Hitachi, Japan).

To prepare TLC-R, the chemical bonds of ChSMA-RGD microspheres were activated with EDC and NHS in an MES (pH = 6.0) buffer. The synthesized TGF-β1@Lipo solution was dispersed in the microsphere solution and shaken overnight. Finally, TLC-R was obtained by centrifugation (ungrafted liposomes remained in the supernatant). The same method was used to produce TLC. To demonstrate the covalent crosslinking of TGF-β1@Lipo with the microspheres, DiO-labelled TGF-β1@Lipo in the TLC-R was first observed by inverted phase-contrast fluorescence microscopy. Then, SEM was used to observe the grafting of TGF-β1@Lipo to the microspheres. FTIR was used to detect the formation of chemical bonds.

2.4. Lubrication properties of TLC-R

Friction experiments were conducted with a universal material testing machine (UMT-4) (Bruker Nano Inc, Germany) to test the COF of

different microspheres (i.e., ChSMA, TLC, and TLC-R) under different loading forces (10 and 15 N). PBS was used as a control. The physiological movement of the knee joint was simulated by mutual friction between the upper (polyethylene ball) and lower (Ti6AI4V) samples. The COF curves over time were recorded during the tests.

2.5. Degradation, encapsulation, and release of TLC-R

To evaluate the degradation performance, different microspheres were immersed in PBS containing 200 U/mL of hyaluronidase (Beijing Laboqi Technology, China) and shaken on a thermostatic shaker. Microspheres were freeze-dried and weighed at predetermined time points, and the degradation line chart was plotted by comparison with the initial weight. The drug encapsulation rate and release kinetics of microspheres containing TGF-β1 were analysed using an enzyme-linked immunosorbent assay (ELISA) kit (eBioscience, USA). To determine the drug encapsulation rate, 1 mL of TGF-β1@Lipo solution was vortexed vigorously to disrupt TGF-β1@Lipo and release TGF-β1. The absorbance at 450 nm was measured. The total drug content (W_t) was calculated. Then, another 1 mL of liposome suspension was centrifuged to separate TGF-β1 from TGF-β1@Lipo. The unencapsulated TGF-β1 drug content (W_u) was detected in the supernatant. Then, W_t and W_u were used to calculate the drug encapsulation rate:

$$\text{Encapsulation rate} = 1 - (W_u / W_t) \times 100\% \quad (1)$$

The encapsulation rate of TLC-R to TGF-β1@Lipo was determined similarly. Simply, the supernatant of ungrafted TGF-β1@Lipo from the previous production of TLC-R was aspirated and vortexed vigorously, and W_u was measured by the ELISA kit. The same mass of TGF-β1@Lipo as that from the production of TLC-R was aspirated and vortexed vigorously, and W_t was measured. Finally, Equation (1) was used to calculate the encapsulation rate of TLC-R to TGF-β1@Lipo.

To determine the drug release from TLC-R, 50 mg of TLC-R was placed in 5 mL of hyaluronidase. All samples were placed in a cell incubator (37 °C, 5 % CO_2). At each time point (days 1, 3, 7, 10, 14, 21, 28, and 35), the supernatant was collected, and the TGF-β1 content was determined by the ELISA kit. The percent cumulative release at each time point was determined by normalizing to the cumulative release of TGF-β1 on day 35. Lipo was placed in PBS and assayed for release by the same method.

2.6. Isolation and cultivation of cells

Chondrocytes were obtained from the hip and knee cartilage of 1-day-old Sprague–Dawley (SD) rats. The rats were first executed by anesthesia, and the femur and tibia were removed. Cartilage was removed from the femur and tibia and cut into pieces. The cartilage was incubated with 0.2 % type II collagenase (Sigma, USA) for 4 h, filtered through a cell sieve, and placed in an incubator (37 °C, 5 % CO_2). Chondrocytes were cultured to the third generation and were frozen for storage. The third-generation cells were identified by a toluidine blue staining solution. In follow-up experiments, 10 ng/mL IL-1β (Peprotech, USA) was applied to mimic the OA inflammatory microenvironment. BMSCs were obtained from the femur and tibia of SD rats aged 6–8 weeks. The primary macrophages were derived from the femur and tibia of C57BL/6 mice aged 6 weeks. The method of extracting and culturing BMSCs and primary macrophages followed the example of previous [38, 39].

2.7. Chondrocyte endocytosis of TGF-β1@Lipo

Chondrocytes with a density of 1×10^5 cells/mL were cultured in a 12-well plate for 8 h. Then, 10 μL of DiI-stained TGF-β1@Lipo was added to the medium. After incubation for 6 h, cells were fixed with 4 % paraformaldehyde (PFA, Beyotime, China) for 20 min, then, stained with Phalloidin (Yeasen, China) for 20 min, and 4,6-diamidino-2-phenylindole (DAPI, Life Tech, USA) for 10 min. They were observed and photographed with an inverted fluorescence microscope.

2.8. Biocompatibility of TLC-R

To evaluate the biocompatibility of the different microspheres, their leachates were obtained by soaking 10 mg/mL of each microsphere in a culture medium, placing the sample in the incubator (37 °C, 5 % CO_2) for 7 days, and collecting the supernatant. The effects on cell viability of different microspheres were detected by live–dead cell staining and cell counting kit-8 (CCK-8) (Beyotime, China). Chondrocytes were cultured in 12-well plates with a density of 1×10^5 cells/mL in a cell culture incubator (37 °C, 5 % CO_2) for 24 h. Then, the chondrocytes were treated with PBS and different microsphere leachates for 1, 2, or 3 days. Chondrocytes were stained with a calcein/PI cell viability/cytotoxicity assay kit (Beyotime, China) and were photographed by an inverted fluorescence microscope. ImageJ was used to quantify the density of living cells.

100 μL of leachate and 10 μL of cell counting CCK-8 solution were added to each well and co-cultured with the chondrocytes for 1, 2, or 3 days. Finally, the supernatant was transferred to a 96-well plate in the dark, and the absorbance at 450 nm was measured.

2.9. Cells recruitment of TLC-R

Pro-inflammatory macrophages were obtained by treating primary macrophages with 100 ng/mL lipopolysaccharide (LPS) (Sigma, USA) for 24 h. The different microspheres were co-incubated with BMSCs and pro-inflammatory macrophages (1×10^5 cells/mL) in anti-adherent 12-well plates for 12 h to evaluate their cell recruitment functions. The cell recruitment properties of the different microspheres were observed by microscopy. For the transwell assay, BMSCs and pro-inflammatory macrophages were added to the upper layer of medium, and different microspheres were added to the lower layer. After incubation at 37 °C for 24 h, migrated cells were stained with 1 % crystal violet (Aladdin, China).

2.10. Chondrogenic induction of TLC-R

To evaluate the chondroinductive ability of the microspheres, BMSCs were incubated with different microsphere leachates for 7 or 14 days. The BMSCs were then fixed with 4 % PFA, stained with 0.1 % Safranin O, and washed with PBS. Finally, the cells were monitored by microscopy.

2.11. Immunofluorescence (IF) staining

Chondrocytes were cultured in 24-well plates at a density of 2.5×10^4 cells/mL and were incubated with 10 ng/mL of IL-1β and the different microsphere leachates for 72 h. The same volume of PBS was added to the control group. After incubation, cells were fixed with 4 % PFA, permeabilized with 0.3 % Triton X-100 (Solarbio, China), and blocked in 5 % BSA (BioSharp, China) for 1 h. After that, the chondrocytes were incubated with rat anti-ACAN and anti-MMP13 (Invitrogen, USA) at 4 °C. One night later, the cells were incubated for 1 h with goat anti-rabbit secondary antibody (Invitrogen, USA). Subsequently, the cytoskeleton was stained with Phalloidin for 20 min, and the nucleus was stained with DAPI for 10 min. An inverted fluorescence microscope was used to take photographs.

2.12. Quantitative real-time polymerase chain reaction (qRT-PCR)

The total RNA of different cells was extracted by TRIzol reagent (Invitrogen, USA). Complementary deoxyribonucleic acid (cDNA) was synthesized using ribonucleic acid (RNA) and PrimeScript RT Master Mix (Takara, Japan). Then, qRT-PCR was performed using a Universal

SYBR Green Supermix (BIO-RAD, USA). The genes were quantified for specific primers using glyceraldehyde 3-phosphate dehydrogenase (GAPDH) as an internal reference (Supplementary Table 1).

2.13. Chondrocyte inflammation inhibition of TLC-R

Chondrocytes at a density of 5×10^4 cells/mL were cultured in six-well plates, and each group was supplemented with 10 ng/mL of IL-1β and different microsphere leachates for 72 h. The concentrations of IL-6 and TNF-α in the cell supernatants were measured with the ELISA kit.

2.14. Flow cytometry assay (FCA)

For the FCA, pro-inflammatory macrophages with a density of 1×10^5 cells/mL were placed in a cell culture incubator (37 °C, 5 % CO_2) for 24 h. They were then incubated for 72 h with different microsphere leachates. After incubation, cells were digested with 0.25 % trypsin, for 10 min and were incubated with the primary antibody (anti-CD11b, anti-CD86, or anti-CD206) for 60 min. The expression of cell surface markers was detected by flow cytometry (CytoFLEX SRT, Thermo Fisher, USA).

2.15. OA animal model construction and microsphere injection

Animal experiments were approved by the Research Ethics Committee of the First Affiliated Hospital of Soochow University (NO. SUDA20231116A04). Male SD rats (12 weeks old) were randomly divided into a control group (6 rats) and an OA group (24 rats). The rats in the OA group were anesthetized with 3 % sodium pentobarbital (40 mg/kg), and the knees were subjected to anterior cruciate ligament transection (ACLT). After surgery, OA rats were further randomized into four groups ($n = 6$) and received 50 μL of an intra-articular injection comprising PBS and 10 mg/L of ChsMA, TLC, or TLC-R. SD rats were euthanized at 4 weeks post-injection, after which knee joints and viscera were removed for analysis.

2.16. Radiological assessment

Eight weeks after ACLT surgery, all rat knees were scanned by enhanced magnetic resonance imaging (MRI) (GE Healthcare, USA), X-ray (Faxitorn Bioptics, USA), and micro-computed tomography (μ-CT) (Bruker, Belgium) imaging. Inflammation and cartilage wear in rat knee joints were evaluated by an animal MRI scanner. Rat knee joints were scanned by an X-ray imager to analyse the joint space widths of the knee joints. Data reconstruction and calculation of TOV were performed using NRecon and CTAn software.

2.17. Histological analysis

Eight weeks after ACLT surgery, the isolated knee joints were fixed in PFA, decalcified, embedded in paraffin, and sectioned. Sagittal sections were stained by hematoxylin and eosin (H&E) and Safranin O–Fast green for histological analysis. The knee pathology was assessed using the Histological score and Osteoarthritis Research Society International (OARSI) scoring system. For immunohistochemical (IHC) staining, the sections were incubated with anti-COL2A1/MMP13/iNOS (Servicebio, China) at 4 °C overnight, followed by incubation with a secondary antibody (Servicebio, China) for 1 h. Then, paraffin sections were stained with 3,3-diaminobenzidine (DAB, Nanjing Jiancheng Bioengineering Institute, China). ImageJ was applied to quantify the levels of COL2A1 and MMP13. The viscera were cryo-embedded, sectioned, and then stained by H&E to assess the *in vivo* biocompatibility of TLC-R.

2.18. In vivo degradation capability of microspheres

TLC-R was immersed in Sulfo-Cy5.5 NHS ester solution (DuoFluor, China) for 1 h for fluorescent labeling. The microspheres were then washed three times with PBS. Then 50 μL of Cy5.5-labelled TLC-R was injected into the knee joint cavity of SD rats. An *in vivo* imaging system (IVIS, Bio Illumination Biotechnology, China) was used to evaluate the retention of microspheres *in vivo*. Fluorescence intensity was measured at 0, 4, 7 and 14 days, respectively.

2.19. Statistical analysis

Statistical analysis was performed with IBM SPSS Statistics version 26 (SPSS Inc., USA). The experimental data of different pairs of groups were compared using Student's t-test. One-or-two-way analysis of variance was performed to compare the experimental data of multiple groups. Results were considered significant when $p < 0.05$.

3. Results

3.1. Preparation and characterization of TLC-R

The hydrogel microspheres ChSMA and ChSMA-RGD were prepared using microfluidic technology. Under a microscope, ChSMA and ChSMA-RGD appeared transparent and homogenous (Fig. 1A). SEM revealed that both ChSMA and ChSMA-RGD possessed a porous structure that provided sufficient surface area for substantial adsorption of drug-loaded liposomes (Fig. 1B). Quantitative analysis indicated that the average diameters of ChSMA and ChSMA-RGD were 114.28 ± 28.19 μm and 121.85 ± 25.31 μm, respectively (Fig. 1C). Lipo was prepared by the thin-film dispersion method, and TEM showed a morphology of homogeneous spheres that remained unchanged after TGF-β1 loading (Fig. 1D). To confirm this, the diameters and zeta potentials of Lipo and TGF-β1@Lipo in ddH_2O were measured by a nanoparticle analyzer. The average diameter of Lipo was 172.73 ± 7.1 nm (PDI: 0.11), while TGF-β1@Lipo (PDI: 0.14) had an average diameter of 177.74 ± 11.95 nm (Fig. 1E, S1A). The zeta potential of the two types of liposomes were −17.5 ± 1.8 mV and −16.8 ± 1.6 mV, respectively. Thus, the size and zeta potential of Lipo and TGF-β1@Lipo remained relatively stable after TGF-β1 loading (Fig. 1F, S1B).

TLC-R was constructed using an amide group to bind TGF-β1@Lipo to ChSMA-RGD or ChSMA microspheres covalently. To confirm the successful production of ChSMA and TLC-R, inverted phase-contrast fluorescence microscopy was used to observe DiO-labelled TGF-β1@Lipo. In contrast to ChsMA, DiO-labelled TGF-β1@Lipo was uniformly dispersed in TLC-R (Fig. 2A). Then, SEM was used to observe ChSMA and TLC-R at high magnification. Both microspheres had a porous structure, and many liposomes were attached within the pores of TLC-R (Fig. 2B). The average diameter of TLC-R was 117.85 ± 24.16 μm, which is similar to that of ChSMA and ChsMA-RGD (Figs. 1C and 2C). FTIR and NMR were used to confirm the formation of chemical bonds, indicating the successful synthesis of ChSMA and the grafting of TGF-β1@Lipo onto ChSMA-RGD. In contrast to ChS, ChSMA, and TLC-R showed visible ester bond peaks at 1719 cm^{-1}, indicating that ester bonds formed between ChS and MA in ChSMA and TLC-R due to esterification. Similarly, NMR found that the characteristic double peaks of MA appeared after grafting, which confirmed that ChSMA was successfully synthesized (Fig. S2). The characteristic peaks of amide bonds were observed in TLC-R at 1651 cm^{-1} (amide I band) and 1557 cm^{-1} (amide II band), which suggests that they formed when TGF-β1@Lipo was grafted onto ChSMA-RGD and confirms that TLC-R was successfully synthesized (Fig. 2D).

The entire degradation process of the microspheres lasted about 35 days, with a total degradation of 91.83 ± 1.45 % (Fig. 2E). Due to the slow degradation of the microspheres, the bearing effect can exist for a longer period of time, as the degradation occurs, more and more liposomes are released, and the articular cartilage is lubricated by hydrated phosphocholine lipids forming a hydrated layer under high loads [34]. The encapsulation rate was calculated to be 87.61 % for liposomes and

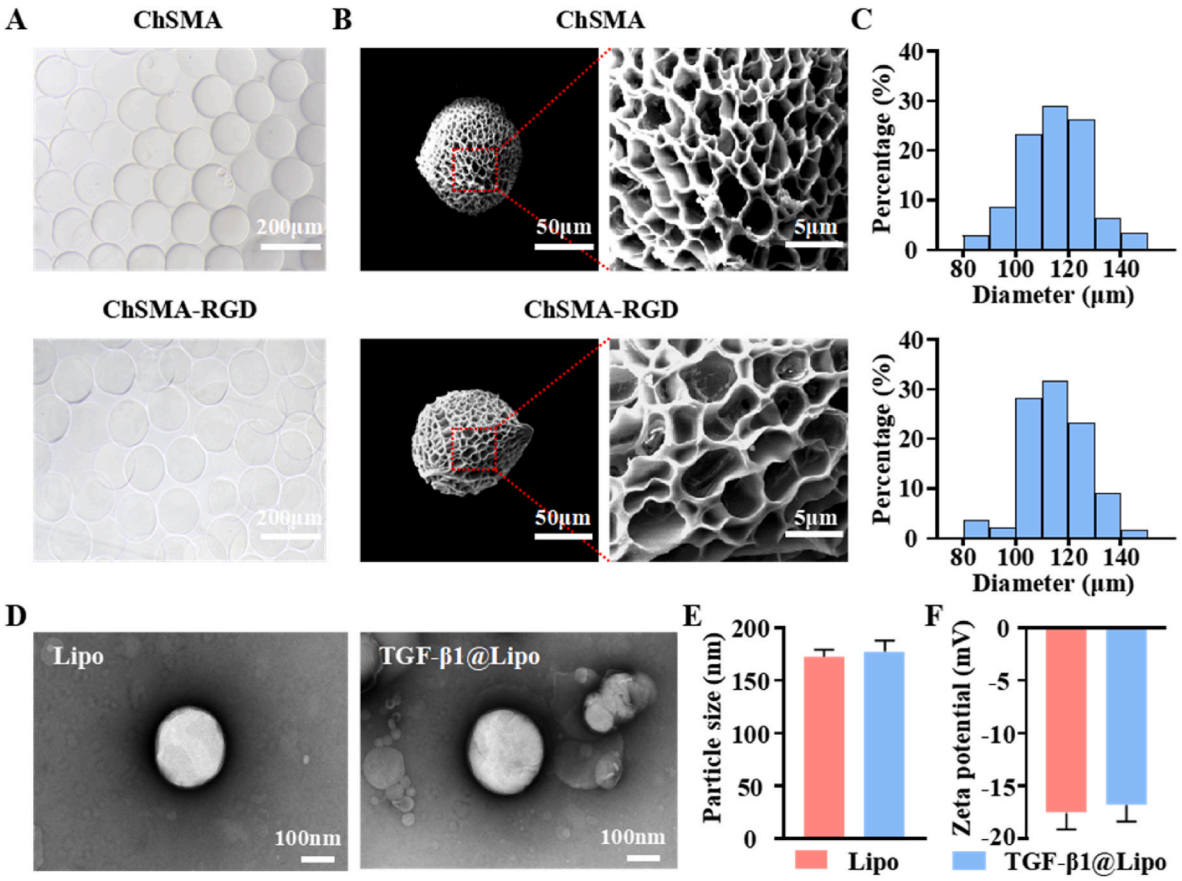

Fig. 1. Characterization of microspheres (ChSMA and ChSMA-RGD) and liposomes (Lipo and TGF-β1@Lipo). **(A)** Microscopic images of ChSMA and ChSMA-RGD microspheres. **(B)** SEM images of ChSMA and ChSMA-RGD microspheres. **(C)** Particle size distributions of ChSMA and ChSMA-RGD microspheres. **(D)** TEM images of Lipo and TGF-β1@Lipo. **(E–F)** Particle size and zeta potential of Lipo and TGF-β1@Lipo.

74.26 % for TLC-R. The release experiment showed that TGF-β1 was slowly released from TLC-R with a total of 90.5 ± 2.2 % released by day 35, but TGF-β1 was quickly released from TGF-β1@Lipo with 74.43 ± 4.33 % released by day 3 and 100 % released by day 7 (Fig. 2F). Thus, the stability of the liposomes was enhanced by covalent bonding to the microspheres, which would allow a single treatment to provide patients with long-lasting therapeutic effects.

OA is a chronic disease characterized by injury to cartilage. Chondrocytes are the primary cell type in cartilage and are heavily involved in the progression of OA, so we extracted chondrocytes for *in vitro* experiments. Chondrocytes extracted from rat cartilage were identified using toluidine blue staining, and they were shown to have a relatively regular morphology with primarily round and oval shapes, clear nuclei, rich cytoplasm, and distinct edges (Fig. S3). This conforms to the typical morphology of normal chondrocytes [40,41]. Cells take up liposomes, which is an important process for the delivery of drugs. Therefore, in order to detect TGF-β1@Lipo endocytosed by chondrocytes, DiI-stained TGF-β1@Lipo was added to the medium, and overlapping fluorescence was observed, which indicated that TGF-β1@Lipo was endocytosed by the chondrocytes (Fig. 2G).

Hydrogel microspheres of uniform small volumes can act as bearings and carry liposomes to maximize their lubricating properties. The COF of different microspheres (i.e., ChSMA, TLC and TLC-R) in PBS was measured by a UMT-4 machine and plotted against time at different loading forces (Fig. S4). TLC-R had the lowest COF under different loads. The COF in the TLC-R group was 0.06 ± 0.01 and 0.05 ± 0.008 at 10 N and 15 N loading force, respectively, which was at least onefold less than the corresponding PBS group (0.12 ± 0.07, 0.12 ± 0.1 respectively), which indicates that TLC-R had good lubricating ability.

3.2. Biocompatibility of TLC-R

The *in vitro* cytotoxicity of different microspheres (i.e., ChSMA, TLC, TLC-R) on chondrocytes was studied by co-culturing the cells with microsphere leachates for 1, 2, or 3 days and conducting cell viability/death assays and CCK-8 experiments. Cell density increased over 3 days for all three microspheres, with few dead cells found (Fig. 3A). Quantitative analysis of the live–dead cell staining showed that the viable cell counts of the TLC-R group on day 3 were 4.98 and 2.08 times higher than on days 1 and 2, respectively. No statistical difference was observed among the three kinds of microspheres over the 3 days (Fig. 3B). The CCK-8 results showed no notable change in cell proliferation activity among the groups at the three time points. On day 3, the control group had an OD of 2.03 ± 0.12, and the TLC-R group had an OD of 1.93 ± 0.25 (Fig. 3C). These results indicate that all three microspheres had good biocompatibility and no cytotoxicity, and they did not affect the proliferation of rat chondrocytes. Thus, they support the potential of TLC-R for clinical application.

3.3. Cells recruitment and chondrogenic differentiation ability of TLC-R in vitro

BMSCs and LPS-treated macrophages (pro-inflammatory macrophages) were co-cultured with different microspheres (i.e., ChSMA, TLC, and TLC-R) for 12 h to observe the cell recruitment ability. BMSCs and pro-inflammatory macrophages were extensively recruited and adhered to TLC-R, while only a few cells adhered to ChSMA and TLC (Fig. 4A). This was likely due to normal cell adhesion behavior during growth. Thus, TLC-R had a robust recruitment ability for BMSCs and pro-

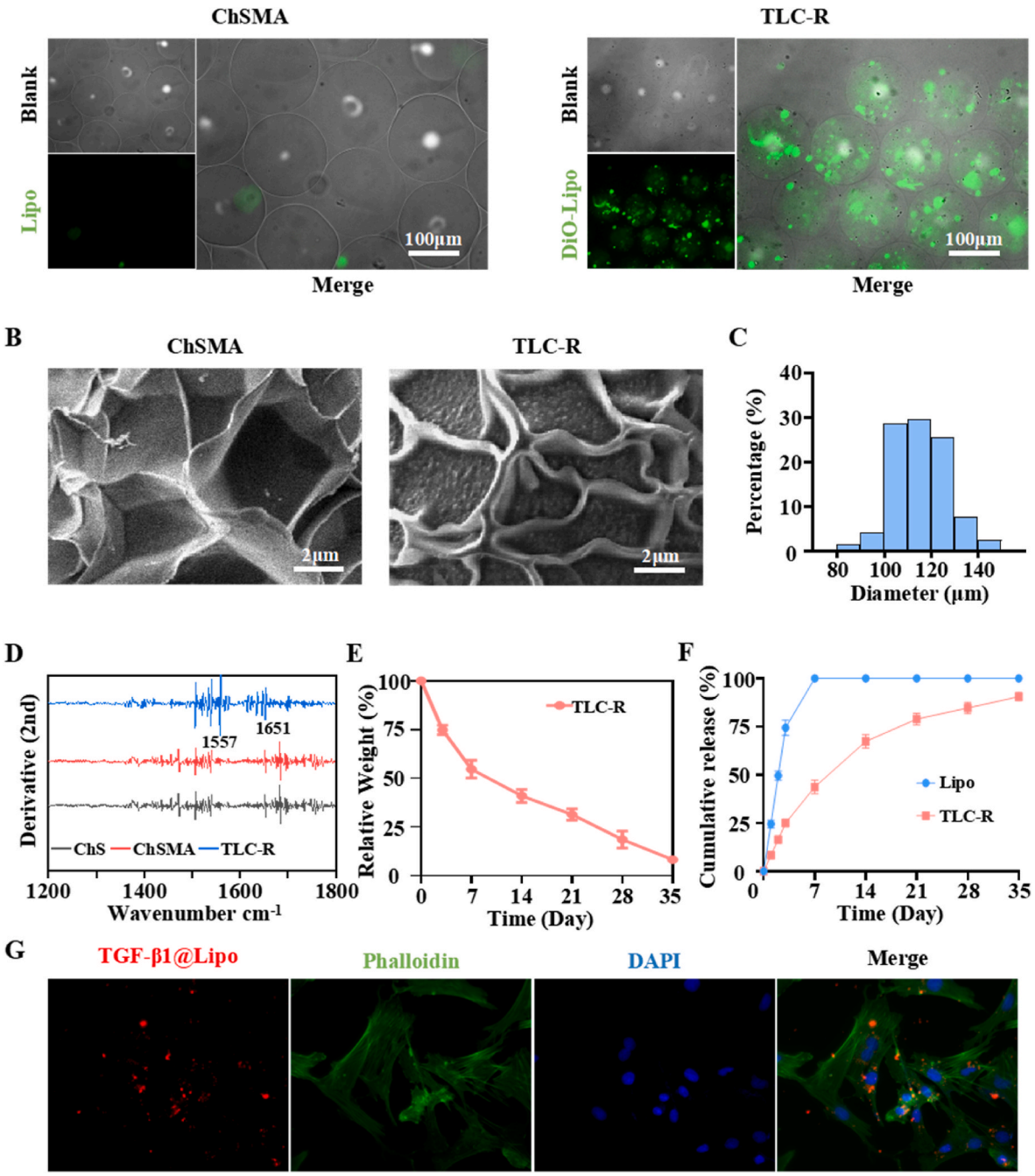

Fig. 2. Characterization of TLC-R. **(A)** Fluorescent micrographs of TLC-R or ChSMA loaded with DiO-stained Lipo. **(B)** SEM images of TLC-R and ChSMA. **(C)** Particle size distribution of TLC-R. **(D)** FTIR results for ChS, ChSMA and TLC-R. **(E)** Degradation rate of TLC-R. **(F)** Cumulative release of TGF-β1 by TGF-β1@Lipo and TLC-R. **(G)** Fluorescent micrographs of TGF-β1@Lipo endocytosed by chondrocytes.

inflammatory macrophages that could be attributed to the presence of RGD peptide.

The leachates of the different microspheres were co-cultured with BMSCs to observe their ability to promote BMSC proliferation and chondrogenic differentiation. After 7 and 14 days, Safranin O staining was applied to monitor morphological changes in BMSCs and secretion of the cartilage matrix. Compared to the control group, all microspheres had some ability to promote chondrogenesis. In particular, BMSCs treated with TLC-R gradually lost their characteristic fibrous structure and began to form monolayer clusters (Fig. 4B). This phenomenon has grown more obvious over time, which indicated the gradual differentiation of BMSCs toward chondrocytes under the effect of ChSMA and TGF-β1. Safranin O staining darkened with increased incubation time, which indicated cell secretion of glycosaminoglycans (GAG) or ChS and can explain the differentiation of BMSCs into chondrocytes. A transwell assay was used to establish a cell-microsphere co-culture system and test the recruitment of BMSCs and pro-inflammatory macrophages by different microspheres. After 24 h, we found that migrating BMSCs and pro-inflammatory macrophages were considerably higher in the RGD-loaded group (TLC-R) than in the ChSMA and TLC groups (Fig. S5).

qRT-PCR was used to detect genes related to cartilage synthesis and metabolism (Col2a1, Sox9, and Acan) in BMSCs after co-culturing with different microsphere leachates for 14 days. The related genes increased by varying degrees with the three microspheres (Fig. 4C). TLC-R was most effective and increased Col2a1, Sox9, and Acan by 14.99, 16.89, and 17.2 times, respectively, compared to the control group. ChSMA and

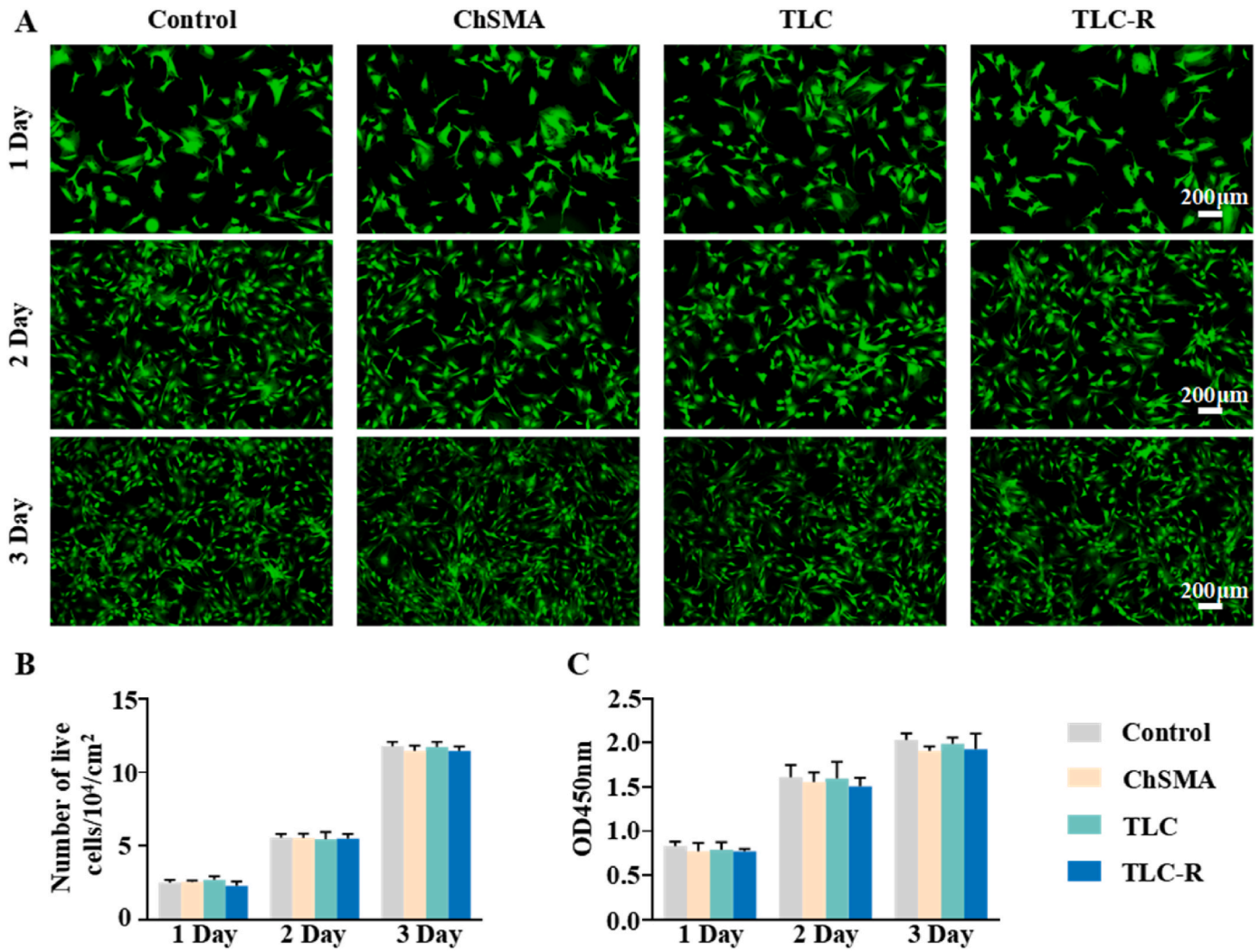

Fig. 3. Biocompatibility of TLC-R. **(A)** Fluorescent micrographs of chondrocytes were obtained by live–dead staining after 1, 2, and 3 days of culturing. **(B)** Quantification of living cells in live–dead staining. **(C)** OD of cell supernatants from CCK-8 assays.

TGF-β1 also played a synergistic role in promoting differentiation. TGF-β1 has been widely used to promote chondrogenic differentiation of BMSCs. However, ChSMA has also been reported to have an effect. A ChSMA concentration of 6 % was found to be best at promoting chondrogenic differentiation of BMSCs, mainly because such a density is optimal for cell interaction [26]. Similarly, ChSMA increased Col2a1, Sox9, and Aca by 5.9, 10.97, and 5.56 times on day 14 compared to the control group.

3.4. Metabolic balance and anti-inflammation of TLC-R in vitro

To assess the metabolic balance of chondrocytes *in vitro*, IF staining and qRT-PCR were used to measure proteins related to synthesis and degradation metabolism and the expression levels of genes. IL-1β is an inflammatory cytokine pivotal in OA, and it was introduced to simulate the inflammatory milieu. The IF staining results showed that the TLC-R group significantly increased the expression of ACAN by 5.56 times compared to the IL-1β group (Fig. 5A and C) and suppressed the expression of MMP13 by 58.72 % (Fig. 5B and D).

The IL-1β group demonstrated a significant reduction in synthesis metabolism-related genes compared to the control group, with 84.08 %, 87.92 %, and 87.16 % in *Col2a1*, *Sox9*, and *Acan,* respectively (Fig. 6A). Genes associated with degradation metabolism increased considerably, with *Adamts4*, *Mmp3*, and *Mmp13* rising by 10.03, 6.34, and 7.45 times, respectively (Fig. 6B). In contrast, the ChSMA, TLC, and TLC-R groups demonstrated significant increases in synthesis metabolism genes and a marked decrease in degradation metabolism genes to varying degrees. In the TLC-R group, *Col2a1*, *Sox9*, and *Acan* increased by 8.18, 7.84, and 10.38 times, respectively, while *Adamts4*, *Mmp3*, and *Mmp13* decreased by 68.15 %, 54.14 %, and 68.92 %, respectively. Notably, the ChSMA group had higher aggregated proteoglycan concentrations than the IL-1β group at both the gene and protein levels (Figs. 5A and 6A) and a lower MMP13 concentration (Figs. 5B and 6B). This phenomenon became more pronounced after TGF-β1@Lipo was introduced, although the difference from TLC-R was insignificant. This suggests that ChSMA and TGF-β1 encapsulated in Lipo synergistically promote the synthesis metabolism of chondrocytes under OA conditions and inhibit degradation metabolism. In summary, the results demonstrated that TLC-R effectively regulates the metabolic balance of chondrocytes in OA inflammatory microenvironment.

To evaluate the impact of the different microspheres on OA inflammatory microenvironment, ELISA kits were employed to detect the expression of relevant proteins. After IL-1β treatment of chondrocytes, TNF-α and IL-6 levels increased significantly by 1.22 times and 64.49 %, respectively. Protein levels decreased after treatment with the three microsphere leachates for 72 h. In particular, the TLC-R group showed a 28.07 % reduction in TNF-α and a 44.77 % reduction in IL-6 (Fig. 6C). Note that there was no significant difference in protein concentrations

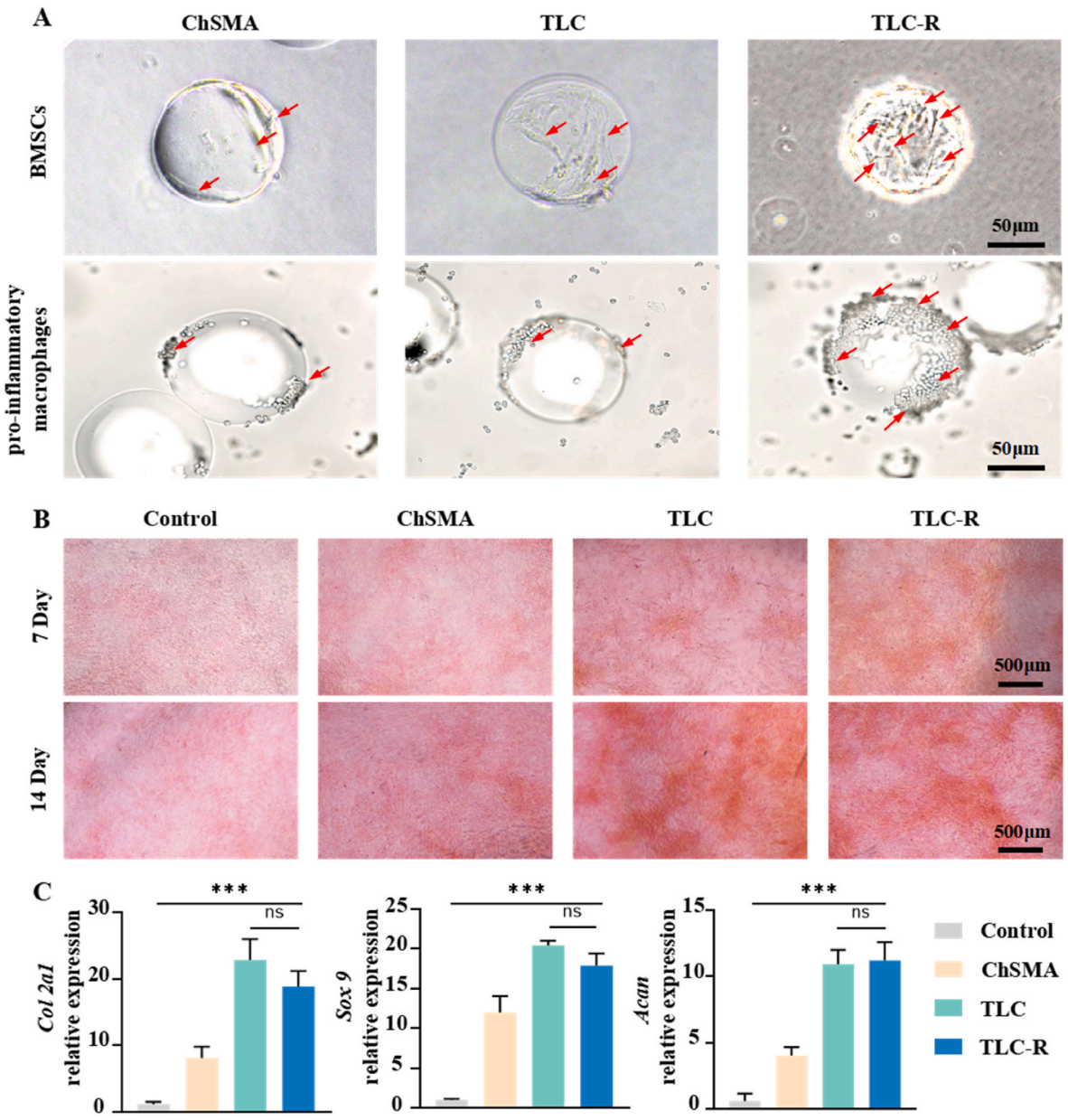

Fig. 4. Cell recruitment and chondrogenic differentiation ability of TLC-R. **(A)** Microscopic images of cell recruitment by different microspheres (i.e., ChSMA, TLC, and TLC-R) when co-incubated with BMSCs and pro-inflammatory macrophages. Some cells are marked with red arrows. **(B)** Safranin O staining results show chondrogenic differentiation of BMSCs under different conditions. **(C)** qRT-PCR results for genes related to cartilage synthesis. ***: $P < 0.001$, ns: no significant difference.

between the three groups, which indicates that all three microspheres could reduce the level of OA inflammation *in vitro*. However, TGF-β1, RGD peptide, and Lipo did not promote nor reduce OA inflammation *in vitro*.

FCA and qRT-PCR were used to evaluate the effect of the different microspheres on OA inflammatory microenvironment based on the impact on pro-inflammatory macrophages. qRT-PCR was used to assess *Inos*, *Tnf-α*, and *IL-1β* levels, representative inflammatory genes of pro-inflammatory macrophages, before and after LPS induction for 24 h. The levels of all three genes significantly increased after LPS induction for 24 h (Fig. S6), which indicates that pro-inflammatory macrophages were successfully induced. Then, FCA was used to study the influence of the different microspheres on the inflammation of the macrophages. Staining was performed to quantify the primary macrophage surface marker (CD11b), pro-inflammatory macrophage surface marker (CD86), and anti-inflammatory macrophage surface marker (CD206) (Fig. 7A). Compared to cells in a typical culture, the $CD86^+/CD11b^+$ ratio after 24 h of LPS induction was 83.53 % ± 6.67 %, indicating that pro-inflammatory macrophages were successfully induced. All microspheres significantly inhibited pro-inflammatory macrophages. In particular, the TLC-R group showed the most notable $CD86^+/CD11b^+$ ratio reduction at 41.02 % (Fig. 7B). However, the $CD206^+/CD11b^+$ ratio did not increase for any groups (Fig. 7C). The qRT-PCR results indicated that all three microspheres reduced the levels of three representative inflammatory genes of pro-inflammatory macrophages. The TLC-R group showed the most significant reductions in *Inos*, *Tnf-α*, and *IL-1β* of 49.78 %, 63.04 %, and 63.15 %, respectively (Fig. 7D–F). The *in vitro* experiments proved that TLC-R could effectively regulate the metabolic balance of chondrocytes in an OA environment and significantly reduce inflammation levels.

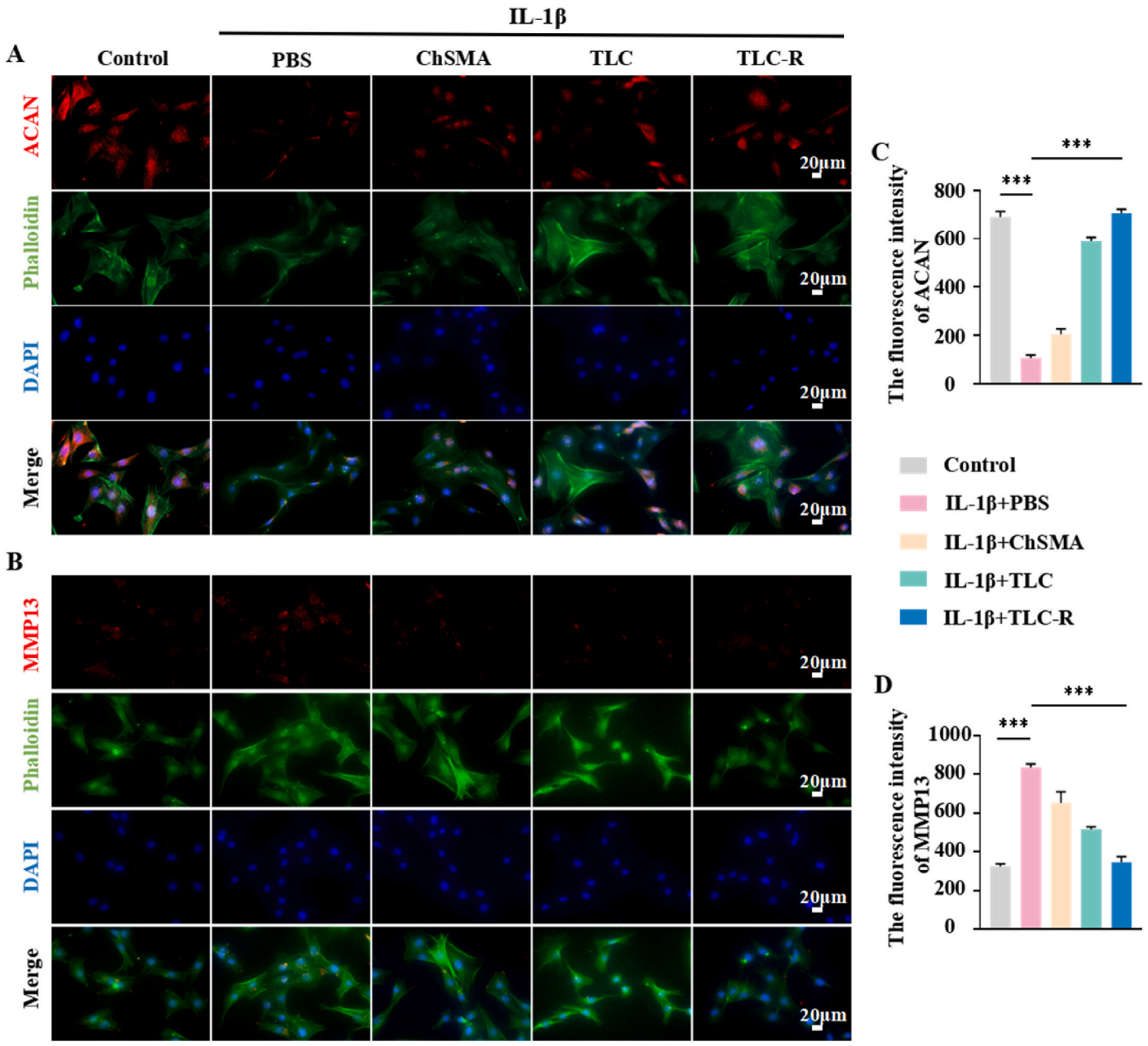

Fig. 5. Effects of different microspheres (i.e., ChSMA, TLC, and TLC-R) on chondrocytes' synthesis and degradation metabolism. **(A, B)** IF staining images of ACAN and MMP13. **(C, D)** Quantitative fluorescence intensities of ACAN and MMP13. ***: $P < 0.001$.

3.5. The therapeutic effect of TLC-R on OA rat in vivo

An OA model was established by ACLT surgery on a 12-week-old SD rat. Four weeks after surgery, PBS or microspheres (i.e., ChSMA, TLC, and TLC-R) were injected intra-articularly. Eight weeks after ACLT surgery, all rats were anesthetized, and their knee joints were evaluated with MRI, which is a standard imaging method for diagnosing OA. MRI can identify early changes in cartilage and synovium to provide a more comprehensive pathological reference [42]. The images revealed significant synovial effusion and severe cartilage erosion in the PBS group. Although some effusion was also present in the TLC-R group, the cartilage maintained a smooth and intact morphology, especially compared to the PBS group (Fig. 8A). Then, the knee joint samples from each group were evaluated more comprehensively by X-ray and μ-CT. The X-ray images indicated a noticeable narrowing of the knee joint space in the PBS group compared to the control group, whereas the TLC-R group showed a significant increase in joint space (Fig. 8B). The PBS group showed a 75.92 % reduction in joint space on average compared to the control group, whereas the TLC-R group showed a 60.82 % increase in joint space on average compared to the PBS group (Fig. 8E). The μ-CT results were used to assess the volume of osteophytes and density of the medial tibial plateau. Compared to the control group, the PBS group showed a significantly thicker subchondral bone for the medial tibial plateau, indicating subchondral bone sclerosis. In contrast, the TLC-R group showed a markedly lower bone density for the medial tibial plateau than the other groups (Fig. 8C). The osteophytes were marked in red and quantified by software (Fig. 8D and F) to observe the total osteophyte volume (TOV) changes between groups. The TLC-R group (TOV: 0.51 ± 0.22 mm^3) and TLC group (TOV: 1.24 ± 0.23 mm^3) had significantly smaller TOVs than the control group, especially the TLC-R group. However, the PBS group had the largest TOV at 2.70 ± 0.11 mm^3. Although ChSMA also reduced the TOV, the effect was suboptimal (TOV: 1.91 ± 0.19 mm^3). These results for the rat OA model confirmed that TLC-R had the best therapeutic effect among the three types of

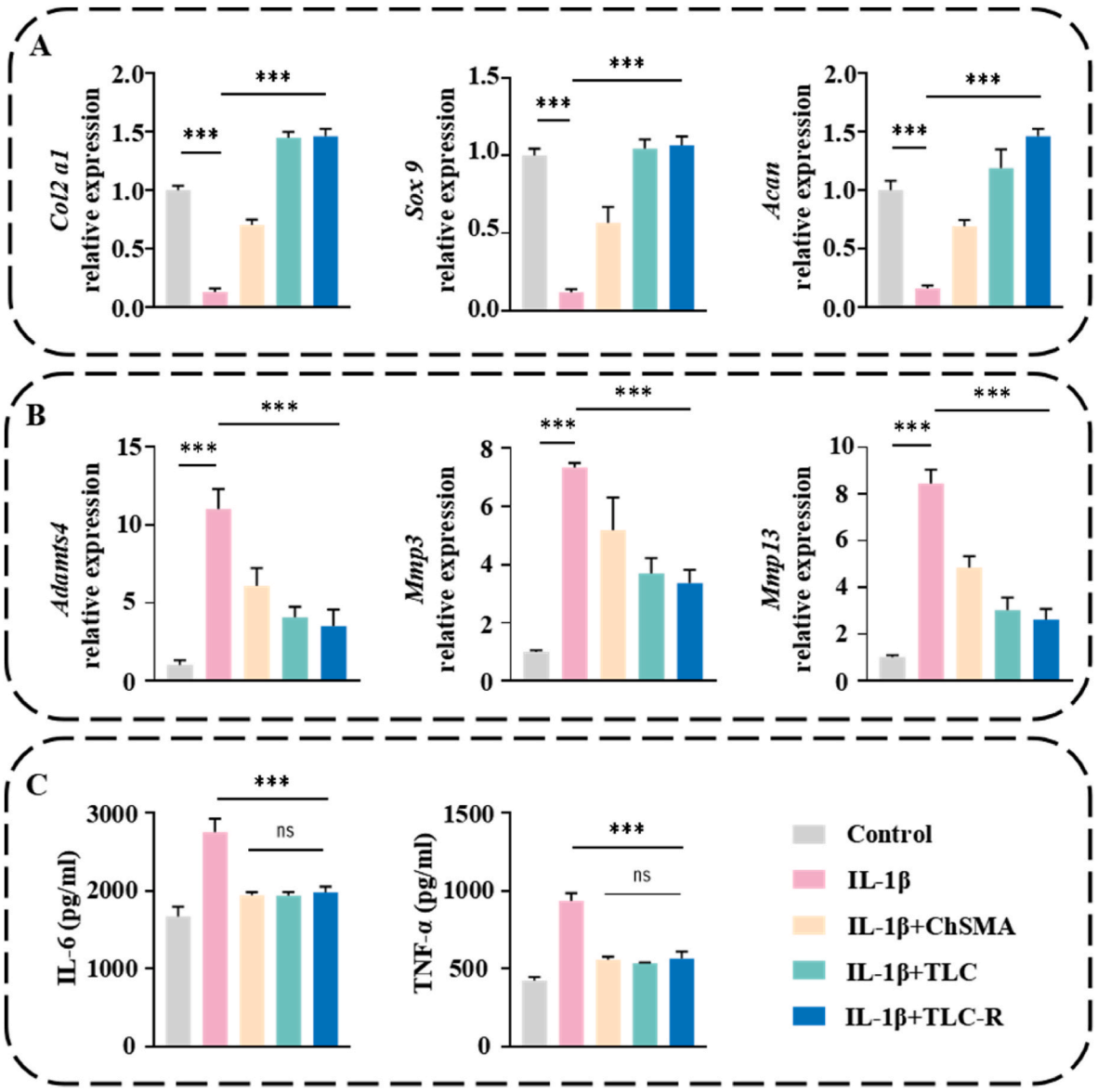

Fig. 6. Effects of different microspheres (i.e., ChSMA, TLC, TLC-R) on inflammatory and metabolic genes or protein concentrations in chondrocytes. **(A)** qRT-PCR results for chondrocyte synthesis metabolism related genes (*Col2a1*, *Sox9*, *Acan*). **(B)** qRT-PCR results for chondrocyte degradation metabolism related genes (*Adamts4*, *Mmp3*, *Mmp13*). **(C)** ELISA results for IL-6 and TNF-α protein concentrations. ***: $P < 0.001$. ns: no significant difference.

microspheres.

H&E staining and Safranin O–fast green staining were applied to evaluate the histology of knee joint tissues. Cartilage fissures, separation, fibrosis, and disordered cell arrangement were observed in the PBS group, which indicates extensive cartilage damage caused by OA accompanied by matrix loss and exposure of the bone surface. In contrast, smooth and even regenerative tissues gradually formed in the TLC-R group, indicating new translucent cartilage formation (Fig. 9A and B). The Krenn synovitis scoring system (Fig. 9C) was used to divide the synovium into three parts for assessment: resident cells, the intimal cell layer, and inflammatory infiltration [43]. The PBS group had significantly higher scores than the control group, which indicates severe damage to the cell morphology, matrix staining, and cartilage appearance. However, all other groups showed varying degrees of improvement. In particular, the TLC-R group had almost the same score as the control group, indicating exceptional therapeutic effects. The OARSI scores reflected the same outcome, the TLC-R group showed an 85 % decrease in its OARSI score at 8 weeks after surgery, while the ChSMA and TLC groups showed decreases of 35.90 % and 69.95 %, respectively (Fig. 9D).

IHC was performed to assess the therapeutic effects of the different microspheres on cartilage metabolic balance. ChSMA and TLC showed increases of 97.82 % and 4.27 times, respectively, in COL2A1 staining compared with the OA group. Meanwhile, TLC-R showed an increase of 5.52 times. In contrast, the PBS group only showed minimal staining compared to the control group (Fig. 10A and C). MMP13 staining was significantly reduced by 66.01 % in the TLC-R group compared with the OA group. The ChSMA and TLC groups also showed less staining than the OA group, but their reductions were more limited at 10.22 % and 38.05 %, respectively (Fig. 10B and D). There was a remarkable increase in iNOS staining in the OA group and a significant decrease in iNOS staining in the ChSMA group by 56.15 % compared to the OA group. The staining in the TLC and TLC-R groups decreased even more, by 66.27 % and 71.01 %, respectively, compared to that in the OA group (Fig. S7). These results indicate that TLC-R improved the cartilage metabolic homeostasis significantly in OA rats and demonstrated marked inhibition of synovial inflammation. To validate the excellent biocompatibility of TLC-R, H&E staining was performed on the heart, liver, spleen, lung, and

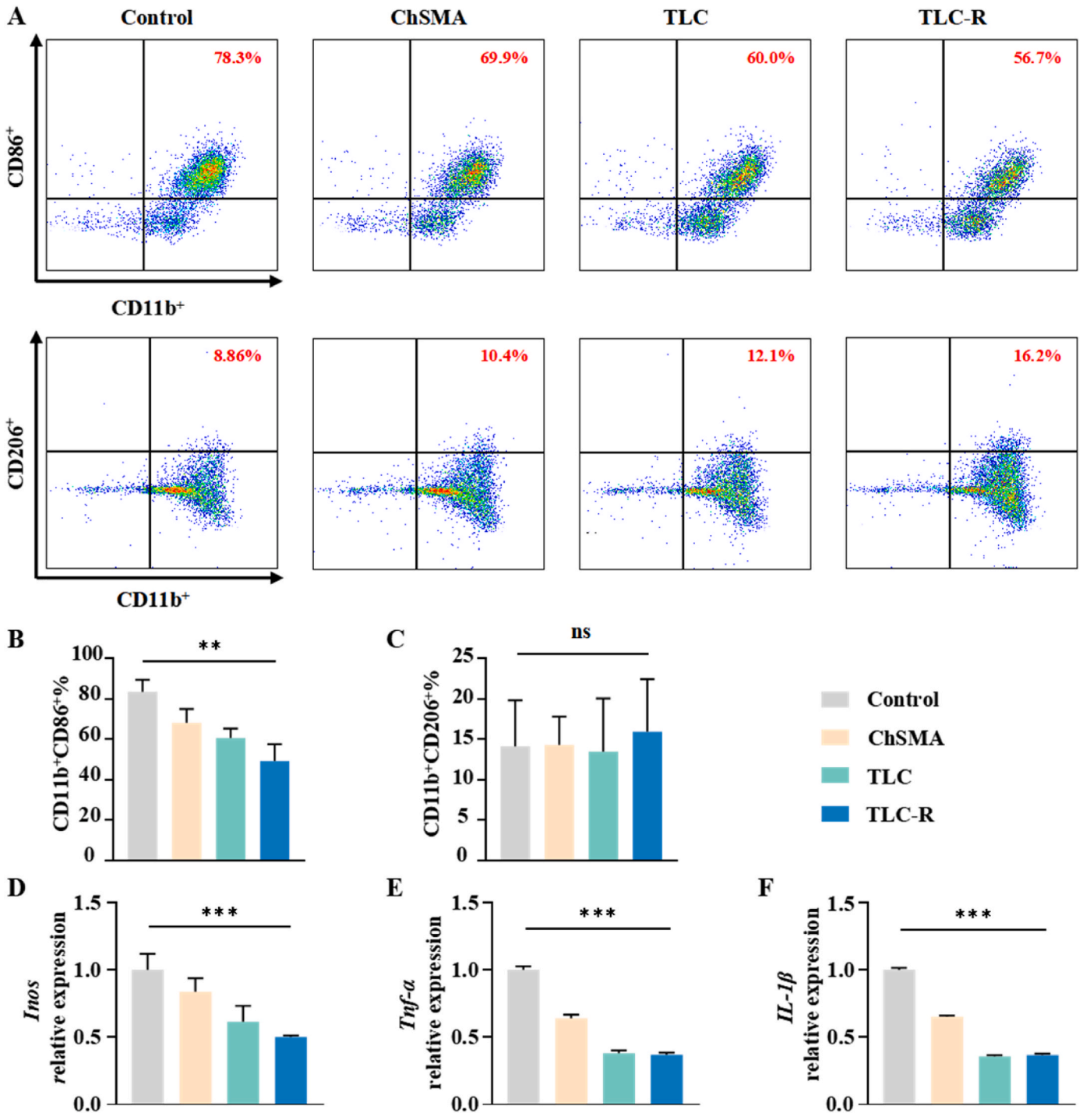

Fig. 7. Effect of different microspheres (i.e., ChSMA, TLC, TLC-R) on pro-inflammatory macrophages. **(A)** FCA results for macrophages. **(B, C)** Quantitative analysis of FCA results. **(D–F)** qRT-PCR results for representative genes of the pro-inflammatory macrophage (*Inos*, *Tnf-α*, and *IL-1β*). **: $P < 0.01$. ***: $P < 0.001$. ns: no significant difference.

kidney tissues of the rats. All groups' cells in the visceral tissues were neatly arranged without hypertrophy, atrophy, abnormal proliferation, or differentiation (Fig. S8). To explore the retention effect of TLC-R in the joint cavity, cy5.5 was loaded onto TLC-R, and the change of fluorescence signal in the joint cavity after surgery was observed by IVIS. On the fourth postoperative day, after intra-articular injection of TLC-R, the fluorescence signal in the joint cavity was maintained at a relatively stable level, and the fluorescence intensity gradually decreased with the gradual degradation of TLC-R. Until the 14th day, a fluorescence signal was still visible in the joint cavity, indicating that TLC-R has an excellent slow-release effect in the joint cavity (Fig. S9).

4. Discussion

The development of OA and cartilage defects is a vicious cycle: catabolic metabolism and pro-inflammatory mediators in OA joints lead to the overproduction of proteolytic enzymes that degrade cartilage, which in turn exacerbates inflammation in the joint. Cartilage is a crucial tissue that reduces friction between bones, so its breakdown may increase friction in the joint and further trigger inflammation and

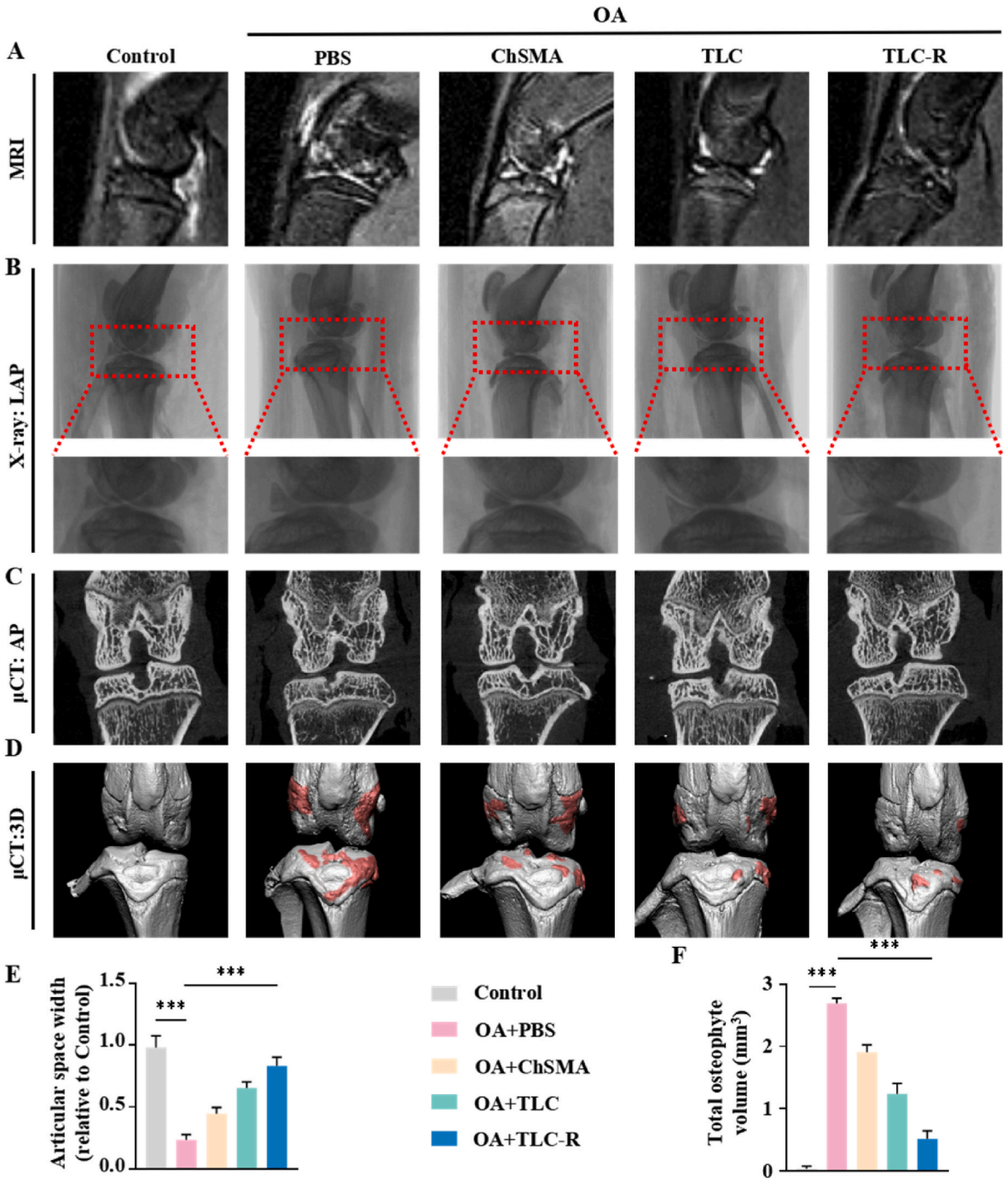

Fig. 8. Effects of injecting different microspheres (i.e., ChSMA, TLC, and TLC-R) on knee joint in SD rat models at 8 weeks after ACLT surgery. **(A)** MRI images. **(B)** X-ray images. **(C, D)** 2D and 3D μ-CT images (osteophytes marked in red). **(E, F)** Quantification of TOV and articular space width. ***: $P < 0.001$.

cartilage defects [44]. Once a cartilage defect occurs, significant regeneration does not occur because of cartilage's complex structure and lack of blood vessels, nerves or lymphatic tissue [45]. Therefore, TLC-R was designed to treat OA by promoting cartilage regeneration, metabolic balance, anti-inflammation and lubrication.

Microspheres can be prepared by microfluidics, batch emulsification, electro-fluid dynamic spraying, and photolithography, and they are easily administered locally through minimally invasive surgery [46,47]. Compared with other technologies, monodisperse microspheres with uniform diameters produced via microfluidics can be achieved by adjusting the flow rate ratio of the oil and water phases. Microspheres of uniform diameter benefit joint cavities because they can act as bearings to assist with lubrication when in contact with the cartilage surface [34]. Liposomes also serve as lubricants. The hydration characteristics of the phospholipid head groups of HSPC form a super-lubricating film on the cartilage surface that effectively reduces the COF in the lesion area, which protects cells from secondary frictional damage and creates favorable conditions for tissue regeneration [48]. Hydrogel microspheres of uniform small volumes can act as bearings and carry liposomes to maximize their lubricating properties. In this study, we covalently bonded TGF-β1@Lipo to ChSMA-RGD via amide linkages to create TLC-R, which combines the lubrication functions of microspheres and liposomes for optimal lubrication performance (Fig. S4). Due to the hydration and lubrication properties of the phospholipid head group of

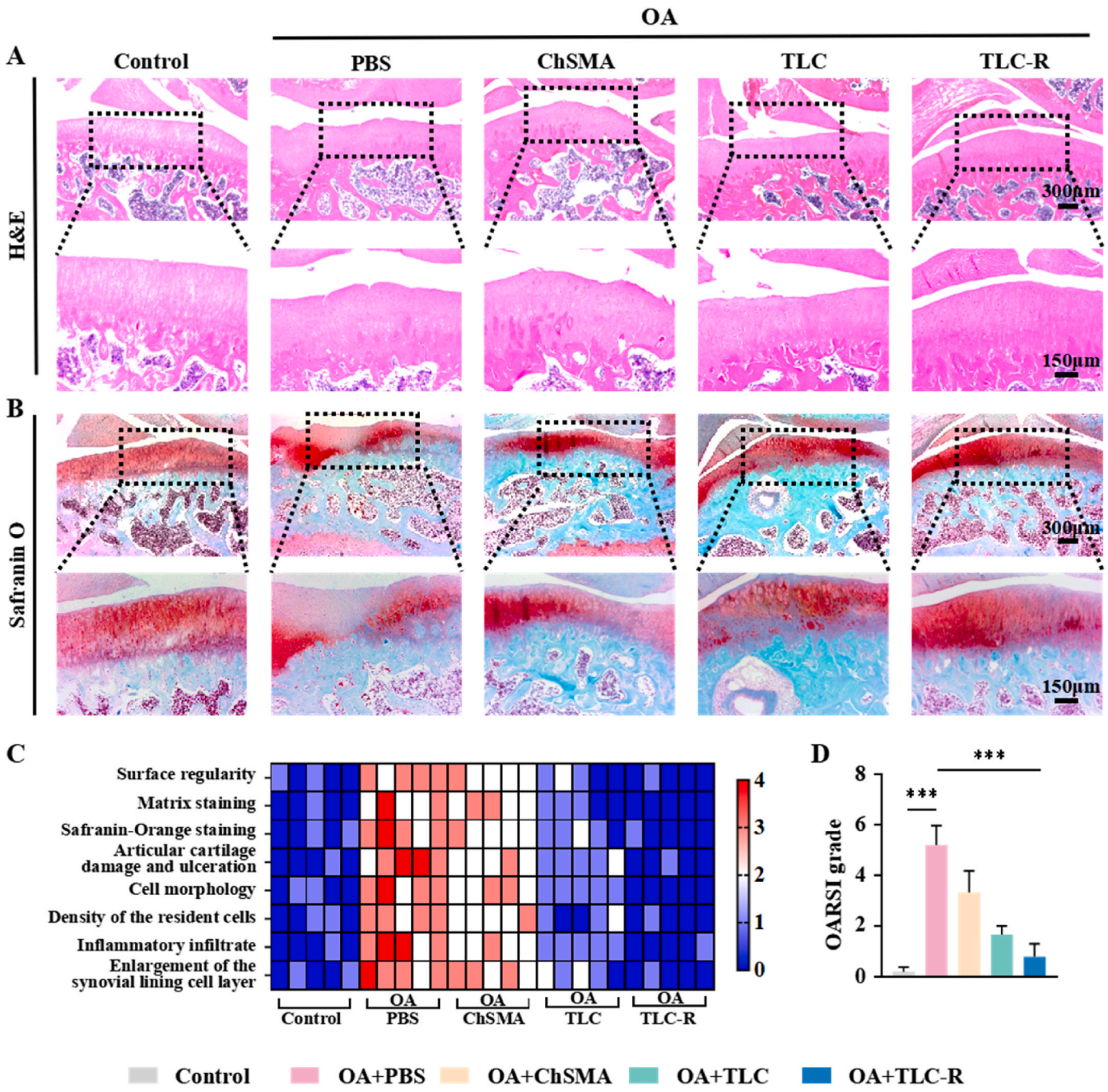

Fig. 9. Histological evaluation of different microspheres (i.e., ChSMA, TLC, and TLC-R) for treating OA in SD rats at 8 weeks after ACLT surgery. **(A, B)** H&E and Safranin O–fast green staining images of SD rat knees. **(C)** Histological and OARSI scores of SD rat knees. ***: $P < 0.001$.

HSPC, a lubricating film will be formed on the surface of the cartilage, which can effectively reduce the COF in the injured area [49]. Interestingly, the COF value of the TLC-R group at 10 N loading force is not higher than that at 15 N loading force or even lower, which may be because the liposomes encapsulated within the microspheres are continuously released to replenish the lubrication layer as the microspheres are worn out to ensure stable lubrication of the microspheres in the long term. TLC-R have the following advantages over commonly reported metal organic framework (MOF) and mesoporous silica spheres: (1) Due to the absence of metal elements, it is more bio-compatible and easier to be biodegraded [50]. (2) Chondroitin sulfate is a glycosaminoglycan, widely found in connective tissues such as cartilage, which regulates the metabolism of chondrocytes, and is more suitable for the treatment of OA. (3) In addition to adsorption, due to the abundance of modifiable chemical bonds, it easier to modify and bind drugs, as well as control drug release [51]. In the present study, we similarly found that TGF-β1 synergistically up regulates anabolic genes and protein levels (Figs. 5A and 6A) and down regulates catabolic genes and proteins (Figs. 5B and 6B) in chondrocytes with ChSMA.

Currently, two methods exist for using hydrogel microspheres to repair cartilage defects. The first method is to encapsulate autologous MSCs within the microspheres and implant them into the defect site [52]. However, this poses several issues. MSCs may lose their pluripotency and self-renewal capacity due to replicative culturing and generation before implantation [53]. The homing ability of MSCs might be reduced due to long-term *in vitro* culturing [5]. Finally, it is challenging

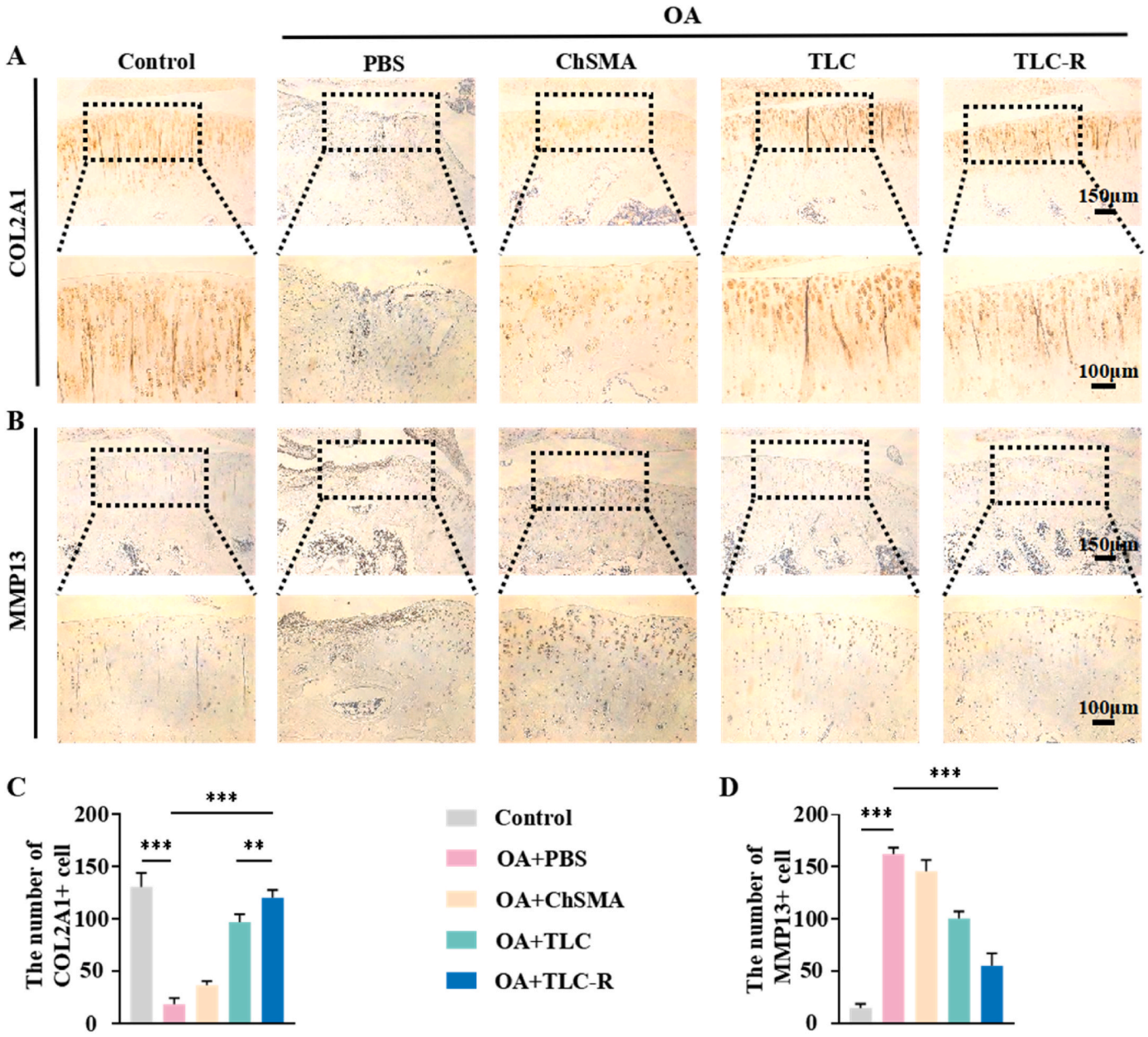

Fig. 10. IHC staining of metabolism-related proteins in rat knee joint sections. **(A, B)** IHC staining images of SD rat knees at 8 weeks after ACLT surgery for COL2A1 and MMP13. **(C, D)** Quantification of IHC for COL2A1 and MMP13. **: $P < 0.01$, ***: $P < 0.001$.

to induce cells to differentiate once implanted [54]. The second method is to assist and induce surrounding autologous stem cells to participate in tissue repair [55,56]. In this study, we found that TLC-R could recruit numerous surrounding BMSCs (Fig. 4A). Under appropriate conditions, BMSCs can be driven toward the chondrocyte lineage. Biological signals such as TGF-β1 are crucial for chondrogenic differentiation of BMSCs induced through the ERK/JNK pathway [57].

Many studies have utilized TGF-β1 to induce MSCs to differentiate into chondrocytes. For example, one study co-cultured MSCs with polymer microspheres loaded with TGF-β1, which induced chondrogenesis *in vitro* by continuously releasing TGF-β1 [58]. When TGF-β1 induces the initial differentiation of BMSCs into chondrocytes, a small amount of COL2A1 is secreted. As chondrogenesis matures, more COL2A1 is secreted along with glycoproteins and transcription factors such as ACAN and SOX9 [59]. In this study, we co-cultured different microsphere leachates (i.e. ChSMA, TLC and TLC-R) with BMSCs *in vitro* for 14 days. The Safranin-O staining results showed that the morphology of BMSCs treated with microspheres carrying TGF-β1 (TLC, TLC-R) gradually changed toward chondrocytes, and the cartilage matrix was secreted in large amounts and turned dark red after 14 days. This indicates that TLC-R promotes the chondrogenic differentiation of BMSCs (Fig. 4B). TGF-β1 is important in cartilage formation and balances chondrocyte metabolism in OA patients. One study used allogeneic human chondrocytes transduced with a retroviral vector to express TGF-β1 to balance chondrocyte metabolism [60]. Clinical trials have used genetically engineered cells to deliver TGF-β1 into damaged cartilage to stimulate cartilage growth by balancing chondrocyte metabolism. The patients all reported improved pain and knee mobility after treatment [61]. This suggests that TGF-β1 is a promising treatment for cartilage lesions.

The binding of RGD peptide to integrin receptors plays a significant role in cell adhesion mechanisms [62]. Previous research has shown that a functionalized hydrogel microsphere (RIBQ) for bone defect repair promotes MSC adhesion and spreading through RGD peptide [63].

Integrins are widely present in many cells, and studies have shown that integrin receptors are highly expressed on the surface of pro-inflammatory macrophages [64,65]. Therefore, while RGD peptide recruits MSCs, it also recruits pro-inflammatory macrophages, which exacerbates inflammation at the diseased site. Most studies focus on only one of the cells, but both MSCs and pro-inflammatory macrophages play important roles in OA. To overcome this 'negative effect', we introduced ChSMA into the drug delivery system so that ChS inhibits inflammation driven by pro-inflammatory macrophages via suppression of NF-κB nuclear translocation [66]. *In vitro* experiments confirmed that TLC-R attracted and adhered to many co-cultured pro-inflammatory macrophages (Fig. 4A). The ACLT model has been demonstrated to induce subchondral bone damage [67], as supported by the evidence presented in our previous study [68]. Consequently, we hypothesize that a subset of the recruited MSCs may originate from the subchondral bone, aligning with the findings reported by Yao et al. [48]. One study implanted E7 (a BMSCs binding peptide)-conjugated polycaprolactone meshes into the knee joints of rats. 7 days after implantation, cells on the mesh were stained with CD44, CD90, and CD105 to investigate the phenotype as BMSCs. The results showed an increase in CD44, CD90, and CD105 positivity of cells attached to and growing into the E7-conjugated polycaprolactone meshes compared to the control group, demonstrating that E7 can recruit BMSCs *in vivo* [69]. Another study showed that RGD-loaded hydrogel scaffolds can recruit MSCs *in vivo*, and they demonstrated its ability to induce MSC differentiation in rat intervertebral discs [70]. In addition, Xiao and his colleagues recruited pro-inflammatory macrophages with hydrogel microspheres incorporating streptavidin proteins and demonstrated *in vivo* that they alleviated inflammation of pro-inflammatory macrophages in the synovium [71]. So, we speculate that RGD peptides with recruitment functions could also recruit MSCs and pro-inflammatory macrophages *in vivo*. Furthermore, because the OA results in a long-term inflammatory microenvironment, we utilized Pep-RGDfkAC, which contains an acrylate group that can be coupled with modified photosensitive biomaterials under the action of photoinitiators with ultraviolet or visible light to tightly link RGD peptide with ChSMA and avoid sudden release of the peptide during degradation and ensure long-term cell recruitment.

Although the *in vivo* and *in vitro* experiments proved the multi-therapeutic effects of TLC-R for OA, this study had several limitations. We did not conduct further mechanistic studies and thus could not assess the specific treatment pathways accurately. When we synthesized TLC-R, we did not explore the effect of the amount of RGD peptide on cell recruitment, so we do not know whether excess RGD peptide would inhibit recruitment. Although the *in vitro* experiments demonstrated the ability of TLC-R to recruit BMSCs and pro-inflammatory macrophages, further investigation is needed to confirm these findings *in vivo*. Finally, other cells are also attracted to RGD peptide because they have the same types of integrins on their surface, but we have only studied two major OA-related cells. The function of RGD peptide on other cells, such as chondrocytes, needs to be explored in the future.

5. Conclusion

We successfully prepared TLC-R, which treats OA by recruiting BMSCs and pro-inflammatory macrophages, suppressing inflammation, enhancing cartilage regeneration, lubrication, and balancing cartilage synthesis and degradation metabolism to treat OA, realizing the function of 'killing two birds with one stone'. The experimental results clearly showed that TLC-R has several noteworthy characteristics: (1) It successfully attracts both MSCs and pro-inflammatory macrophages thanks to the presence of RGD peptide. (2) It has excellent anti-inflammatory, cartilage regeneration, and balancing cartilage synthesis and degradation metabolism effects thanks to ChS and TGF-β1. (3) It exhibits exceptional lubrication effects owing to the uniformly sized microspheres acting as ball bearings combined with the lubrication capabilities of liposomes. TLC-R proves that modifying multi-functional hydrogel microspheres with RGD peptide can realize an effective and comprehensive OA treatment.

CRediT authorship contribution statement

Yun Zhou: Writing – review & editing, Writing – original draft, Visualization, Validation. **Xu He:** Visualization, Validation, Methodology, Investigation. **Wen Zhang:** Supervision, Software, Resources. **Weiguo Zhang:** Resources, Formal analysis, Conceptualization. **Huan Zhao:** Supervision, Data curation, Conceptualization. **Xichao Zhou:** Validation, Supervision, Investigation. **Qiaoli Gu:** Supervision, Formal analysis. **Hao Shen:** Investigation, Conceptualization. **Huilin Yang:** Funding acquisition, Formal analysis, Conceptualization. **Xingzhi Liu:** Writing – review & editing, Supervision, Methodology, Conceptualization. **Lixin Huang:** Resources, Funding acquisition, Formal analysis. **Qin Shi:** Project administration, Funding acquisition, Formal analysis, Conceptualization.

Declaration of competing interest

The authors declare that they have no known competing financial interests or personal relationships that could have appeared to influence the work reported in this paper.

Data availability

Data will be made available on request.

Acknowledgements

This work was supported by grants from the National Natural Science Foundation of China (82372457, 82172485), Technology Innovation on Medicine and Health of Suzhou Science and Technology Bureau (SKY2022041), the Orthopaedic Medical Innovation Center of Jiangsu (CXZX202209), Key Laboratory of Orthopaedics of Suzhou (SZS2022017), the Priority Academic Program Development of Jiangsu Higher Education Institutions (PAPD), Jiangsu Funding Program for Excellent Postdoctoral Talent (2023ZB202). Jiangsu Provincial Traditional Chinese Medicine Science and Technology Development Project (No. ZD202232).

Appendix A. Supplementary data

Supplementary data to this article can be found online at https://doi.org/10.1016/j.mtbio.2024.101127.

References

[1] Q. Yao, X. Wu, C. Tao, W. Gong, M. Chen, M. Qu, et al., Osteoarthritis: pathogenic signaling pathways and therapeutic targets, Signal Transduct. Targeted Ther. 8 (1) (2023) 56.
[2] D.J. Hunter, L. March, M. Chew, Osteoarthritis in 2020 and beyond: a Lancet Commission, Lancet 396 (10264) (2020) 1711–1712.
[3] X.L. Yuan, H.Y. Meng, Y.C. Wang, J. Peng, Q.Y. Guo, A.Y. Wang, et al., Bone-cartilage interface crosstalk in osteoarthritis: potential pathways and future therapeutic strategies, Osteoarthritis Cartilage 22 (8) (2014) 1077–1089.
[4] D. Zhang, Y. Su, P. Sun, X. Liu, L. Zhang, X. Ling, et al., A TGF-loading hydrogel scaffold capable of promoting chondrogenic differentiation for repairing rabbit nasal septum cartilage defect, Front. Bioeng. Biotechnol. 10 (2022) 1057904.
[5] W.J. Rombouts, R.E. Ploemacher, Primary murine MSC show highly efficient homing to the bone marrow but lose homing ability following culture, Leukemia 17 (1) (2003) 160–170.
[6] A.E. Rapp, R. Bindl, A. Erbacher, A. Kruchen, M. Rojewski, H. Schrezenmeier, et al., Autologous mesenchymal stroma cells are superior to allogeneic ones in bone defect regeneration, Int. J. Mol. Sci. 19 (9) (2018) 2526.
[7] M. van den Bosch, Osteoarthritis year in review 2020: biology, Osteoarthritis Cartilage 29 (2) (2021) 143–150.
[8] J. Van den Bossche, J. Baardman, N.A. Otto, S. van der Velden, A.E. Neele, S.M. van den Berg, et al., Mitochondrial dysfunction prevents repolarization of inflammatory macrophages, Cell Rep. 17 (3) (2016) 684–696.

[9] L. He, J.H. Jhong, Q. Chen, K.Y. Huang, K. Strittmatter, J. Kreuzer, et al., Global characterization of macrophage polarization mechanisms and identification of M2-type polarization inhibitors, Cell Rep. 37 (5) (2021) 109955.
[10] S. Culemann, A. Gruneboom, J.A. Nicolas-Avila, D. Weidner, K.F. Lammle, T. Rothe, et al., Locally renewing resident synovial macrophages provide a protective barrier for the joint, Nature 572 (7771) (2019) 670–675.
[11] K. Knab, D. Chambers, G. Kronke, Synovial macrophage and fibroblast heterogeneity in joint homeostasis and inflammation, Front. Med. 9 (2022) 862161.
[12] B.G. Cooper, B. Catalina, A. Nazarian, B.D. Snyder, M.W. Grinstaff, Active agents, biomaterials, and technologies to improve biolubrication and strengthen soft tissues, Biomaterials 181 (2018) 210–226.
[13] M. Yang, Z.C. Zhang, Y. Liu, Y.R. Chen, R.H. Deng, Z.N. Zhang, et al., Function and mechanism of RGD in bone and cartilage tissue engineering, Front. Bioeng. Biotechnol. 9 (2021) 773636.
[14] Z. Yang, H. Li, Z. Yuan, L. Fu, S. Jiang, C. Gao, et al., Endogenous cell recruitment strategy for articular cartilage regeneration, Acta Biomater. 114 (2020) 31–52.
[15] Q. Wang, K. Onuma, C. Liu, H. Wong, M.S. Bloom, E.E. Elliott, et al., Dysregulated integrin alphaVbeta3 and CD47 signaling promotes joint inflammation, cartilage breakdown, and progression of osteoarthritis, Jci Insight 4 (18) (2019).
[16] C. Deng, Q. Zhang, P. He, B. Zhou, K. He, X. Sun, et al., Targeted apoptosis of macrophages and osteoclasts in arthritic joints is effective against advanced inflammatory arthritis, Nat. Commun. 12 (1) (2021) 2174.
[17] L. Diao, B. Meibohm, Pharmacokinetics and pharmacokinetic-pharmacodynamic correlations of therapeutic peptides, Clin. Pharmacokinet. 52 (10) (2013) 855–868.
[18] Z. Wang, L. Dong, L. Han, K. Wang, X. Lu, L. Fang, et al., Self-assembled biodegradable nanoparticles and polysaccharides as biomimetic ECM nanostructures for the synergistic effect of RGD and BMP-2 on bone formation, Sci. Rep. 6 (2016) 25090.
[19] M. Sandor, A. Riechel, I. Kaplan, E. Mathiowitz, Effect of lecithin and MgCO3 as additives on the enzymatic activity of carbonic anhydrase encapsulated in poly (lactide-co-glycolide) (PLGA) microspheres, Biochim. Biophys. Acta 1570 (1) (2002) 63–74.
[20] Y. Qiao, X. Liu, X. Zhou, H. Zhang, W. Zhang, W. Xiao, et al., Gelatin templated polypeptide Co-Cross-Linked hydrogel for bone regeneration, Adv. Healthcare Mater. 9 (1) (2020) e1901239.
[21] X. Ju, X. Liu, Y. Zhang, X. Chen, M. Chen, H. Shen, Y. Feng, J. Liu, M. Wang, Q. Shi, A photo-crosslinked proteinogenic hydrogel endogenous TGF-β1 for cartilage regeneration, Smart Materials in Medicine 3 (2022) 85–93.
[22] W. Wei, Y. Ma, X. Yao, W. Zhou, X. Wang, C. Li, et al., Advanced hydrogels for the repair of cartilage defects and regeneration, Bioact. Mater. 6 (4) (2021) 998–1011.
[23] P. Angele, J. Abke, R. Kujat, H. Faltermeier, D. Schumann, M. Nerlich, et al., Influence of different collagen species on physico-chemical properties of crosslinked collagen matrices, Biomaterials 25 (14) (2004) 2831–2841.
[24] H. Wang, Z. Meng, C.Y. Zhao, Y.H. Xiao, H. Zeng, H. Lian, et al., Research progress of implantation materials and its biological evaluation, Biomed. Mater. 18 (6) (2023) 062001.
[25] A. Grossman, P.J. Moult, D. Cunnah, M. Besser, Different opioid mechanisms are involved in the modulation of ACTH and gonadotrophin release in man, Neuroendocrinology 42 (4) (1986) 357–360.
[26] C. Ai, L. Liu, K. Wong, X.H. Tan, J. Goh, The effect of chondroitin sulfate concentration and matrix stiffness on chondrogenic differentiation of mesenchymal stem cells, Biomater. Sci. 11 (13) (2023) 4557–4573.
[27] J.M. Coburn, M. Gibson, S. Monagle, Z. Patterson, J.H. Elisseeff, Bioinspired nanofibers support chondrogenesis for articular cartilage repair, Proc. Natl. Acad. Sci. U.S.A. 109 (25) (2012) 10012–10017.
[28] P.A. Levett, F.P. Melchels, K. Schrobback, D.W. Hutmacher, J. Malda, T.J. Klein, A biomimetic extracellular matrix for cartilage tissue engineering centered on photocurable gelatin, hyaluronic acid and chondroitin sulfate, Acta Biomater. 10 (1) (2014) 214–223.
[29] X. Li, Q. Xu, M. Johnson, X. Wang, J. Lyu, Y. Li, et al., A chondroitin sulfate based injectable hydrogel for delivery of stem cells in cartilage regeneration, Biomater. Sci. 9 (11) (2021) 4139–4148.
[30] E.A. Aisenbrey, S.J. Bryant, The role of chondroitin sulfate in regulating hypertrophy during MSC chondrogenesis in a cartilage mimetic hydrogel under dynamic loading, Biomaterials 190–191 (2019) 51–62.
[31] D.A. Wang, S. Varghese, B. Sharma, I. Strehin, S. Fermanian, J. Gorham, et al., Multifunctional chondroitin sulphate for cartilage tissue-biomaterial integration, Nat. Mater. 6 (5) (2007) 385–392.
[32] L.J. Baier, K.A. Bivens, C.J. Patrick, C.E. Schmidt, Photocrosslinked hyaluronic acid hydrogels: natural, biodegradable tissue engineering scaffolds, Biotechnol. Bioeng. 82 (5) (2003) 578–589.
[33] Y. He, M. Sun, J. Wang, X. Yang, C. Lin, L. Ge, et al., Chondroitin sulfate microspheres anchored with drug-loaded liposomes play a dual antioxidant role in the treatment of osteoarthritis, Acta Biomater. 151 (2022) 512–527.
[34] J. Yang, Y. Han, J. Lin, Y. Zhu, F. Wang, L. Deng, et al., Ball-bearing-Inspired polyampholyte-modified microspheres as bio-lubricants attenuate osteoarthritis, Small 16 (44) (2020) e2004519.
[35] J. Tan, J. Li, X. Zhou, Generation of cell-laden GelMA microspheres using microfluidic chip and its cryopreservation method, Biomed. Mater. 18 (5) (2023) 055023.
[36] R. Cheng, L. Liu, Y. Xiang, Y. Lu, L. Deng, H. Zhang, et al., Advanced liposome-loaded scaffolds for therapeutic and tissue engineering applications, Biomaterials 232 (2020) 119706.
[37] R. Rudge, J. van de Sande, J.A. Dijksman, E. Scholten, Uncovering friction dynamics using hydrogel particles as soft ball bearings, Soft Matter 16 (15) (2020) 3821–3831.
[38] Y. Huang, Y. Yin, Y. Gu, Q. Gu, H. Yang, Z. Zhou, et al., Characterization and immunogenicity of bone marrow-derived mesenchymal stem cells under osteoporotic conditions, Sci. China Life Sci. 63 (3) (2020) 429–442.
[39] M. Chen, Y. Zhang, P. Zhou, X. Liu, H. Zhao, X. Zhou, et al., Substrate stiffness modulates bone marrow-derived macrophage polarization through NF-kappaB signaling pathway, Bioact. Mater. 5 (4) (2020) 880–890.
[40] A. Gartland, J. Mechler, A. Mason-Savas, C.A. MacKay, G. Mailhot, S.J. Marks, et al., In vitro chondrocyte differentiation using costochondral chondrocytes as a source of primary rat chondrocyte cultures: an improved isolation and cryopreservation method, Bone 37 (4) (2005) 530–544.
[41] A.C. Hall, The role of chondrocyte morphology and volume in controlling phenotype-implications for osteoarthritis, cartilage repair, and cartilage engineering, Curr. Rheumatol. Rep. 21 (8) (2019) 38.
[42] J.N. Katz, K.R. Arant, R.F. Loeser, Diagnosis and treatment of hip and knee osteoarthritis: a review, JAMA, J. Am. Med. Assoc. 325 (6) (2021) 568–578.
[43] V. Krenn, L. Morawietz, G.R. Burmester, R.W. Kinne, U. Mueller-Ladner, B. Muller, et al., Synovitis score: discrimination between chronic low-grade and high-grade synovitis, Histopathology 49 (4) (2006) 358–364.
[44] D. Sun, X. Liu, L. Xu, Y. Meng, H. Kang, Z. Li, Advances in the treatment of partial-thickness cartilage defect, Int. J. Nanomed. 17 (2022) 6275–6287.
[45] Z. Zhou, J. Cui, S. Wu, Z. Geng, J. Su, Silk fibroin-based biomaterials for cartilage/osteochondral repair, Theranostics 12 (11) (2022) 5103–5124.
[46] Q. Pan, W. Su, Y. Yao, Progress in microsphere-based scaffolds in bone/cartilage tissue engineering, Biomed. Mater. 18 (6) (2023) 062004.
[47] K.A. El, Green and functional aerogels by macromolecular and textural engineering of chitosan microspheres, Chem. Rec. 20 (8) (2020) 753–772.
[48] Y. Yao, G. Wei, L. Deng, W. Cui, Visualizable and lubricating hydrogel microspheres via NanoPOSS for cartilage regeneration, Adv. Sci. 10 (15) (2023) e2207438.
[49] W. Lin, M. Kluzek, N. Iuster, E. Shimoni, N. Kampf, R. Goldberg, et al., Cartilage-inspired, lipid-based boundary-lubricated hydrogels, Science 370 (6514) (2020) 335–338.
[50] C. Schuurmans, M. Mihajlovic, C. Hiemstra, K. Ito, W.E. Hennink, T. Vermonden, Hyaluronic acid and chondroitin sulfate (meth)acrylate-based hydrogels for tissue engineering: synthesis, characteristics and pre-clinical evaluation, Biomaterials 268 (2021) 120602.
[51] K.Y. Wong, Z. Nie, M.S. Wong, Y. Wang, J. Liu, Metal-drug coordination nanoparticles and hydrogels for enhanced delivery, Adv. Mater. (2024) e2404053.
[52] H. Tan, D. Huang, L. Lao, C. Gao, RGD modified PLGA/gelatin microspheres as microcarriers for chondrocyte delivery, J. Biomed. Mater. Res. B Appl. Biomater. 91 (1) (2009) 228–238.
[53] K. Ksiazek, A comprehensive review on mesenchymal stem cell growth and senescence, Rejuvenation Res. 12 (2) (2009) 105–116.
[54] I. Urlic, A. Ivkovic, Cell sources for cartilage repair-biological and clinical perspective, Cells 10 (9) (2021).
[55] T. Guo, M. Noshin, H.B. Baker, E. Taskoy, S.J. Meredith, Q. Tang, et al., 3D printed biofunctionalized scaffolds for microfracture repair of cartilage defects, Biomaterials 185 (2018) 219–231.
[56] B. Sharma, S. Fermanian, M. Gibson, S. Unterman, D.A. Herzka, B. Cascio, et al., Human cartilage repair with a photoreactive adhesive-hydrogel composite, Sci. Transl. Med. 5 (167) (2013) 167ra6.
[57] X. Jiang, B. Huang, H. Yang, G. Li, C. Zhang, G. Yang, et al., TGF-beta1 is involved in vitamin D-induced chondrogenic differentiation of bone marrow-derived mesenchymal stem cells by regulating the ERK/JNK pathway, Cell. Physiol. Biochem. 42 (6) (2017) 2230–2241.
[58] L.D. Solorio, A.S. Fu, R. Hernandez-Irizarry, E. Alsberg, Chondrogenic differentiation of human mesenchymal stem cell aggregates via controlled release of TGF-beta1 from incorporated polymer microspheres, J. Biomed. Mater. Res. 92 (3) (2010) 1139–1144.
[59] M. Demoor, D. Ollitrault, T. Gomez-Leduc, M. Bouyoucef, M. Hervieu, H. Fabre, et al., Cartilage tissue engineering: molecular control of chondrocyte differentiation for proper cartilage matrix reconstruction, Biochim. Biophys. Acta 1840 (8) (2014) 2414–2440.
[60] C.W. Ha, M.J. Noh, K.B. Choi, K.H. Lee, Initial phase I safety of retrovirally transduced human chondrocytes expressing transforming growth factor-beta-1 in degenerative arthritis patients, Cytotherapy 14 (2) (2012) 247–256.
[61] C.W. Ha, J.J. Cho, R.K. Elmallah, J.J. Cherian, T.W. Kim, M.C. Lee, et al., A multicenter, single-blind, phase IIa clinical trial to evaluate the efficacy and safety of a cell-mediated gene therapy in degenerative knee arthritis patients, Human Gene Therapy Clinical Development 26 (2) (2015) 125–130.
[62] U. Hersel, C. Dahmen, H. Kessler, RGD modified polymers: biomaterials for stimulated cell adhesion and beyond, Biomaterials 24 (24) (2003) 4385–4415.
[63] Q. Li, H. Zhang, Z. Zeng, S. Yan, Y. Hei, Y. Zhang, et al., Functionalized hydrogel-microsphere composites stimulating neurite outgrowth for vascularized bone regeneration, Biomater. Sci. 11 (15) (2023) 5274–5286.
[64] S.K. Ramaiah, S. Rittling, Pathophysiological role of osteopontin in hepatic inflammation, toxicity, and cancer, Toxicol. Sci. 103 (1) (2008) 4–13.
[65] I. Van Hove, T.T. Hu, K. Beets, T. Van Bergen, I. Etienne, A.W. Stitt, et al., Targeting RGD-binding integrins as an integrative therapy for diabetic retinopathy and neovascular age-related macular degeneration, Prog. Retin. Eye Res. 85 (2021) 100966.

[66] S. Hatano, H. Watanabe, Regulation of macrophage and dendritic cell function by chondroitin sulfate in innate to antigen-specific adaptive immunity, Front. Immunol. 11 (2020) 232.
[67] A.M. Bendele, Animal models of osteoarthritis, J. Musculoskelet. Neuronal Interact. 1 (4) (2001) 363–376.
[68] K. Miao, Y. Zhou, X. He, Y. Xu, X. Zhang, H. Zhao, et al., Microenvironment-responsive bilayer hydrogel microspheres with gelatin-shell for osteoarthritis treatment, Int. J. Biol. Macromol. 261 (Pt 2) (2024) 129862.
[69] Z. Shao, X. Zhang, Y. Pi, X. Wang, Z. Jia, J. Zhu, et al., Polycaprolactone electrospun mesh conjugated with an MSC affinity peptide for MSC homing in vivo, Biomaterials 33 (12) (2012) 3375–3387.
[70] C.Y. Ho, C.C. Wang, T.C. Wu, C.H. Kuan, Y.C. Liu, T.W. Wang, Peptide-functionalized double network hydrogel with compressible shape memory effect for intervertebral disc regeneration, Bioengineering & Translational Medicine 8 (2) (2023) e10447.
[71] P. Xiao, X. Han, Y. Huang, J. Yang, L. Chen, Z. Cai, et al., Reprogramming macrophages via immune cell mobilized hydrogel microspheres for osteoarthritis treatments, Bioact. Mater. 32 (2024) 242–259.